SEARCHES FOR GRAVITATIONAL WAVES FROM KNOWN PULSARS WITH SCIENCE RUN 5 LIGO DATA

SEARCHES FOR GRAVITATIONAL WAVES FROM KNOWN PULSARS WITH SCIENCE RUN 5 LIGO DATA

B. P. Abbott[1], R. Abbott[1], F. Acernese[2ac], R. Adhikari[1], P. Ajith[3], B. Allen[3,4], G. Allen[5], M. Alshourbagy[6ab],
R. S. Amin[7], S. B. Anderson[1], W. G. Anderson[4], F. Antonucci[8a], S. Aoudia[9a], M. A. Arain[10], M. Araya[1], H. Armandula[1],
P. Armor[4], K. G. Arun[11], Y. Aso[1], S. Aston[12], P. Astone[8a], P. Aufmuth[13], C. Aulbert[3], S. Babak[14], P. Baker[15],
G. Ballardin[16], S. Ballmer[1], C. Barker[17], D. Barker[17], F. Barone[2ac], B. Barr[18], P. Barriga[19], L. Barsotti[20],
M. Barsuglia[21], M. A. Barton[1], I. Bartos[22], R. Bassiri[18], M. Bastarrika[18], Th. S. Bauer[23a], B. Behnke[14], M. Beker[23],
M. Benacquista[24], J. Betzwieser[1], P. T. Beyersdorf[25], S. Bigotta[6ab], I. A. Bilenko[26], G. Billingsley[1], S. Birindelli[9a],
R. Biswas[4], M. A. Bizouard[11], E. Black[1], J. K. Blackburn[1], L. Blackburn[20], D. Blair[19], B. Bland[17], C. Boccara[27],
T. P. Bodiya[20], L. Bogue[28], F. Bondu[9b], L. Bonelli[6ab], R. Bork[1], V. Boschi[1], S. Bose[29], L. Bosi[30a], S. Braccini[6a],
C. Bradaschia[6a], P. R. Brady[4], V. B. Braginsky[26], J. E. Brau[31], D. O. Bridges[28], A. Brillet[9a], M. Brinkmann[3],
V. Brisson[11], C. Van Den Broeck[32], A. F. Brooks[1], D. A. Brown[33], A. Brummit[34], G. Brunet[20], R. Budzyński[35b],
T. Bulik[35cd], A. Bullington[5], H. J. Bulten[23ab], A. Buonanno[36], O. Burmeister[3], D. Buskulic[37], R. L. Byer[5],
L. Cadonati[38], G. Cagnoli[39a], E. Calloni[2ab], J. B. Camp[40], E. Campagna[39ac], J. Cannizzo[40], K. C. Cannon[1], B. Canuel[16],
J. Cao[20], F. Carbognani[16], L. Cardenas[1], S. Caride[41], G. Castaldi[42], S. Caudill[7], M. Cavaglià[43], F. Cavalier[11],
R. Cavalieri[16], G. Cella[6a], C. Cepeda[1], E. Cesarini[39c], T. Chalermsongsak[1], E. Chalkley[18], P. Charlton[44],
E. Chassande-Mottin[21], S. Chatterji[1], S. Chelkowski[12], Y. Chen[14,45], A. Chincarini[46], N. Christensen[47],
C. T. Y. Chung[48], D. Clark[5], J. Clark[32], J. H. Clayton[4], F. Cleva[9a], E. Coccia[49ab], T. Cokelaer[32], C. N. Colacino[6,50],
J. Colas[16], A. Colla[8ab], M. Colombini[8b], R. Conte[2c], D. Cook[17], T. R. C. Corbitt[20], C. Corda[6ab], N. Cornish[15], A. Corsi[8a],
J.-P. Coulon[9a], D. Coward[19], D. C. Coyne[1], J. D. E. Creighton[4], T. D. Creighton[24], A. M. Cruise[12], R. M. Culter[12],
A. Cumming[18], L. Cunningham[18], E. Cuoco[16], S. L. Danilishin[26], S. D'Antonio[49a], K. Danzmann[3,13], A. Dari[30ab],
V. Dattilo[16], B. Daudert[1], M. Davier[11], G. Davies[32], E. J. Daw[51], R. Day[16], R. De Rosa[2ab], D. DeBra[5], J. Degallaix[3],
M. DEL PRETE[6ac], V. Dergachev[41], S. Desai[52], R. DeSalvo[1], S. Dhurandhar[53], L. Di Fiore[2a], A. Di Lieto[6ab],
M. Di Paolo Emilio[49ad], A. Di Virgilio[6a], M. Díaz[24], A. Dietz[32,37], F. Donovan[20], K. L. Dooley[10], E. E. Doomes[54],
M. Drago[55cd], R. W. P. Drever[56], J. Dueck[3], I. Duke[20], J.-C. Dumas[19], J. G. Dwyer[22], C. Echols[1], M. Edgar[18], A. Effler[17],
P. Ehrens[1], E. Espinoza[1], T. Etzel[1], M. Evans[20], T. Evans[28], V. Fafone[49ab], S. Fairhurst[32], Y. Faltas[10], Y. Fan[19], D. Fazi[1],
H. Fehrmann[3], I. Ferrante[6ab], F. Fidecaro[6ab], L. S. Finn[52], I. Fiori[16], R. Flaminio[57], K. Flasch[4], S. Foley[20], C. Forrest[58],
N. Fotopoulos[4], J.-D. Fournier[9a], J. Franc[57], A. Franzen[13], S. Frasca[8ab], F. Frasconi[6a], M. Frede[3], M. Frei[59], Z. Frei[50],
A. Freise[12], R. Frey[31], T. Fricke[28], P. Fritschel[20], V. V. Frolov[28], M. Fyffe[28], V. Galdi[42], L. Gammaitoni[30ab],
J. A. Garofoli[33], F. Garufi[2ab], G. Gemme[46], E. Genin[16], A. Gennai[6a], I. Gholami[14], J. A. Giaime[7,28], S. Giampanis[3],
K. D. Giardina[28], A. Giazotto[6a], K. Goda[20], E. Goetz[41], L. M. Goggin[4], G. González[7], M. L. Gorodetsky[26], S. Gossler[3,23],
R. Gouaty[7], M. Granata[21], V. Granata[37], A. Grant[18], S. Gras[19], C. Gray[17], M. Gray[60], R. J. S. Greenhalgh[34],
A. M. Gretarsson[61], C. Greverie[9a], F. Grimaldi[20], R. Grosso[24], H. Grote[3], S. Grunewald[14], M. Guenther[17], G. Guidi[39ac],
E. K. Gustafson[1], R. Gustafson[41], B. Hage[13], J. M. Hallam[12], D. Hammer[4], G. D. Hammond[18], C. Hanna[1], J. Hanson[28],
J. Harms[62], G. M. Harry[20], I. W. Harry[32], E. D. Harstad[31], K. Haughian[18], K. Hayama[24], J. Heefner[1], H. Heitmann[9],
P. Hello[11], I. S. Heng[18], A. Heptonstall[1], M. Hewitson[3], S. Hild[12], E. Hirose[33], D. Hoak[28], K. A. Hodge[1], K. Holt[28],
D. J. Hosken[63], J. Hough[18], D. Hoyland[19], D. Huet[16], B. Hughey[20], S. H. Huttner[18], D. R. Ingram[17], T. Isogai[47], M. Ito[31],
A. Ivanov[1], P. Jaranowski[35e], B. Johnson[17], W. W. Johnson[7], D. I. Jones[64], G. Jones[32], R. Jones[18], L. Sancho de la
Jordana[65], L. Ju[19], P. Kalmus[1], V. Kalogera[66], S. Kandhasamy[62], J. Kanner[36], D. Kasprzyk[12], E. Katsavounidis[20],
K. Kawabe[17], S. Kawamura[67], F. Kawazoe[3], W. Kells[1], D. G. Keppel[1], A. Khalaidovski[3], F. Y. Khalili[26], R. Khan[22],
E. Khazanov[68], P. King[1], J. S. Kissel[7], S. Klimenko[10], K. Kokeyama[67], V. Kondrashov[1], R. Kopparapu[52], S. Koranda[4],
I. Kowalska[35c], D. Kozak[1], B. Krishnan[14], A. Królak[35af], R. Kumar[18], P. Kwee[13], P. La Penna[16], P. K. Lam[60],
M. Landry[17], B. Lantz[5], A. Lazzarini[1], H. Lei[24], M. Lei[1], N. Leindecker[5], I. Leonor[31], N. Leroy[11], N. Letendre[37], C. Li[45],
H. Lin[10], P. E. Lindquist[1], T. B. Littenberg[15], N. A. Lockerbie[69], D. Lodhia[12], M. Longo[42], M. Lorenzini[39a], V. Loriette[27],
M. Lormand[28], G. Losurdo[39a], P. Lu[5], M. Lubinski[17], A. Lucianetti[10], H. Lück[3,13], B. Machenschalk[14], M. MacInnis[20],
J.-M. Mackowski[57], M. Mageswaran[1], K. Mailand[1], E. Majorana[8a], N. Man[9a], I. Mandel[66], V. Mandic[62],
M. Mantovani[6c], F. Marchesoni[30a], F. Marion[37], S. Márka[22], Z. Márka[22], A. Markosyan[5], J. Markowitz[20], E. Maros[1],
J. Marque[16], F. Martelli[39ac], I. W. Martin[18], R. M. Martin[10], J. N. Marx[1], K. Mason[20], A. Masserot[37], F. Matichard[7],
L. Matone[22], R. A. Matzner[59], N. Mavalvala[20], R. McCarthy[17], D. E. McClelland[60], S. C. McGuire[54], M. McHugh[70],
G. McIntyre[1], D. J. A. McKechan[32], K. McKenzie[60], M. Mehmet[3], A. Melatos[48], A. C. Melissinos[58], G. Mendell[17],
D. F. Menéndez[52], F. Menzinger[16], R. A. Mercer[4], S. Meshkov[1], C. Messenger[3], M. S. Meyer[28], C. Michel[57],
L. Milano[2ab], J. Miller[18], J. Minelli[52], Y. Minenkov[49a], Y. Mino[45], V. P. Mitrofanov[26], G. Mitselmakher[10],
R. Mittleman[20], O. Miyakawa[1], B. Moe[4], M. Mohan[16], S. D. Mohanty[24], S. R. P. Mohapatra[38], J. Moreau[27],
G. Moreno[17], N. Morgado[57], A. Morgia[49ab], T. Morioka[67], K. Mors[3], S. Mosca[2ab], V. Moscatelli[8a], K. Mossavi[3],
B. Mours[37], C. MowLowry[60], G. Mueller[10], D. Muhammad[28], H. zur Mühlen[13], S. Mukherjee[24], H. Mukhopadhyay[53],
A. Mullavey[60], H. Müller-Ebhardt[3], J. Munch[63], P. G. Murray[18], E. Myers[17], J. Myers[17], T. Nash[1], J. Nelson[18],
I. Neri[30ab], G. Newton[18], A. Nishizawa[67], F. Nocera[16], K. Numata[40], E. Ochsner[36], J. O'Dell[34], G. H. Ogin[1],

B. O'Reilly[28], R. O'Shaughnessy[52], D. J. Ottaway[63], R. S. Ottens[10], H. Overmier[28], B. J. Owen[52], G. Pagliaroli[49ad],
C. Palomba[8a], Y. Pan[36], C. Pankow[10], F. Paoletti[6a,16], M. A. Papa[14,4], V. Parameshwaraiah[17], S. Pardi[2ab],
A. Pasqualetti[16], R. Passaquieti[6ab], D. Passuello[6a], P. Patel[1], M. Pedraza[1], S. Penn[71], A. Perreca[12], G. Persichetti[2ab],
M. Pichot[9a], F. Piergiovanni[39ac], V. Pierro[42], M. Pietka[35e], L. Pinard[57], I. M. Pinto[42], M. Pitkin[18], H. J. Pletsch[3],
M. V. Plissi[18], R. Poggiani[6ab], F. Postiglione[2c], M. Prato[46], M. Principe[42], R. Prix[3], G. A. Prodi[55ab], L. Prokhorov[26],
O. Puncken[3], M. Punturo[30a], P. Puppo[8a], V. Quetschke[10], F. J. Raab[17], O. Rabaste[21], D. S. Rabeling[23ab], H. Radkins[17],
P. Raffai[50], Z. Raics[22], N. Rainer[3], M. Rakhmanov[24], P. Rapagnani[8ab], V. Raymond[66], V. Re[55ab], C. M. Reed[17], T. Reed[72],
T. Regimbau[9a], H. Rehbein[3], S. Reid[18], D. H. Reitze[10], F. Ricci[8ab], R. Riesen[28], K. Riles[41], B. Rivera[17], P. Roberts[73],
N. A. Robertson[1,18], F. Robinet[11], C. Robinson[32], E. L. Robinson[14], A. Rocchi[49a], S. Roddy[28], L. Rolland[37], J. Rollins[22],
J. D. Romano[24], R. Romano[2ac], J. H. Romie[28], D. Rosińska[35dg], C. Röver[3], S. Rowan[18], A. Rüdiger[3], P. Ruggi[16], P. Russell[1],
K. Ryan[17], S. Sakata[67], F. Salemi[55ab], V. Sandberg[17], V. Sannibale[1], L. Santamaría[14], S. Saraf[74], P. Sarin[20],
B. Sassolas[57], B. S. Sathyaprakash[32], S. Sato[67], M. Satterthwaite[60], P. R. Saulson[33], R. Savage[17], P. Savov[45],
M. Scanlan[72], R. Schilling[3], R. Schnabel[3], R. Schofield[31], B. Schulz[3], B. F. Schutz[14,32], P. Schwinberg[17], J. Scott[18],
S. M. Scott[60], A. C. Searle[1], B. Sears[1], F. Seifert[3], D. Sellers[28], A. S. Sengupta[1], D. Sentenac[16], A. Sergeev[68],
B. Shapiro[20], P. Shawhan[36], D. H. Shoemaker[20], A. Sibley[28], X. Siemens[4], D. Sigg[17], S. Sinha[5], A. M. Sintes[65],
B. J. J. Slagmolen[60], J. Slutsky[7], M. V. van der Sluys[66], J. R. Smith[33], M. R. Smith[1], N. D. Smith[20], K. Somiya[45],
B. Sorazu[18], A. Stein[20], L. C. Stein[20], S. Steplewski[29], A. Stochino[1], R. Stone[24], K. A. Strain[18], S. Strigin[26],
A. Stroeer[40], R. Sturani[39ac], A. L. Stuver[28], T. Z. Summerscales[73], K. -X. Sun[5], M. Sung[7], P. J. Sutton[32], B. Swinkels[16],
G. P. Szokoly[50], D. Talukder[29], L. Tang[24], D. B. Tanner[10], S. P. Tarabrin[26], J. R. Taylor[3], R. Taylor[1], R. Terenzi[49ac],
J. Thacker[28], K. A. Thorne[28], K. S. Thorne[45], A. Thüring[13], K. V. Tokmakov[18], A. Toncelli[6ab], M. Tonelli[6ab], C. Torres[28],
C. Torrie[1], E. Tournefier[37], F. Travasso[30ab], G. Traylor[28], M. Trias[65], J. Trummer[37], D. Ugolini[75], J. Ulmen[5],
K. Urbanek[5], H. Vahlbruch[13], G. Vajente[6ab], M. Vallisneri[45], J. F. J. van den Brand[23ab], S. van der Putten[23a], S. Vass[1],
R. Vaulin[4], M. Vavoulidis[11], A. Vecchio[12], G. Vedovato[55c], A. A. van Veggel[18], J. Veitch[12], P. Veitch[63], C. Veltkamp[3],
D. Verkindt[37], F. Vetrano[39ac], A. Viceré[39ac], A. Villar[1], J.-Y. Vinet[9a], H. Vocca[30a], C. Vorvick[17], S. P. Vyachanin[26],
S. J. Waldman[20], L. Wallace[1], R. L. Ward[1], M. Was[11], A. Weidner[3], M. Weinert[3], A. J. Weinstein[1], R. Weiss[20],
L. Wen[19,45], S. Wen[7], K. Wette[60], J. T. Whelan[14,76], S. E. Whitcomb[1], B. F. Whiting[10], C. Wilkinson[17], P. A. Willems[1],
H. R. Williams[52], L. Williams[10], B. Willke[3,13], I. Wilmut[34], L. Winkelmann[3], W. Winkler[3], C. C. Wipf[20], A. G. Wiseman[4],
G. Woan[18], R. Wooley[28], J. Worden[17], W. Wu[10], I. Yakushin[28], H. Yamamoto[1], Z. Yan[19], S. Yoshida[77], M. Yvert[37],
M. Zanolin[61], J. Zhang[41], L. Zhang[1], C. Zhao[19], N. Zotov[72], M. E. Zucker[20], J. Zweizig[1]

(The LIGO Scientific Collaboration & The Virgo Collaboration)

S. Bégin[78,79], A. Corongiu[80], N. D'Amico[80,81], P. C. C. Freire[82,83], J. W. T. Hessels[84,85], G. B. Hobbs[86], M. Kramer[87],
A. G. Lyne[87], R. N. Manchester[86], F. E. Marshall[40], J. Middleditch[88], A. Possenti[80], S. M. Ransom[89], I. H. Stairs[78],

and

B. Stappers[87]

[1] LIGO-California Institute of Technology, Pasadena, CA 91125, USA
[2] INFN, aSezione di Napoli; bUniversità di Napoli "Federico II" Complesso Universitario di Monte S. Angelo, I-80126 Napoli; cUniversità di Salerno, Fisciano,
I-84084 Salerno, Italy
[3] Albert-Einstein-Institut, Max-Planck-Institut für Gravitationsphysik, D-30167 Hannover, Germany
[4] University of Wisconsin-Milwaukee, Milwaukee, WI 53201, USA
[5] Stanford University, Stanford, CA 94305, USA
[6] INFN, aSezione di Pisa; bUniversità di Pisa; I-56127 Pisa; cUniversità di Siena, I-53100 Siena, Italy
[7] Louisiana State University, Baton Rouge, LA 70803, USA
[8] INFN, aSezione di Roma; bUniversità "La Sapienza", I-00185 Roma, Italy
[9] aDepartement Artemis, Observatoire de la Côte d'Azur, CNRS, F-06304 Nice; bInstitut de Physique de Rennes, CNRS, Université de Rennes 1,
35042 Rennes; France
[10] University of Florida, Gainesville, FL 32611, USA
[11] LAL, Université Paris-Sud, IN2P3/CNRS, F-91898 Orsay, France
[12] University of Birmingham, Birmingham B15 2TT, UK
[13] Leibniz Universität Hannover, D-30167 Hannover, Germany
[14] Albert-Einstein-Institut, Max-Planck-Institut für Gravitationsphysik, D-14476 Golm, Germany
[15] Montana State University, Bozeman, MT 59717, USA
[16] European Gravitational Observatory (EGO), I-56021 Cascina (Pi), Italy
[17] LIGO-Hanford Observatory, Richland, WA 99352, USA
[18] University of Glasgow, Glasgow G12 8QQ, UK
[19] University of Western Australia, Crawley, WA 6009, Australia
[20] LIGO-Massachusetts Institute of Technology, Cambridge, MA 02139, USA
[21] AstroParticule et Cosmologie (APC), CNRS: UMR7164-IN2P3-Observatoire de Paris-Université Denis Diderot-Paris VII-CEA: DSM/IRFU, France
[22] Columbia University, New York, NY 10027, USA
[23] aNikhef, National Institute for Subatomic Physics, P.O. Box 41882, 1009 DB; bVU University Amsterdam, De Boelelaan 1081, 1081 HV;
Amsterdam, The Netherlands
[24] The University of Texas at Brownsville and Texas Southmost College, Brownsville, TX 78520, USA
[25] San Jose State University, San Jose, CA 95192, USA
[26] Moscow State University, Moscow 119992, Russia
[27] ESPCI, CNRS, F-75005 Paris, France
[28] LIGO-Livingston Observatory, Livingston, LA 70754, USA
[29] Washington State University, Pullman, WA 99164, USA

[30] INFN, [a]Sezione di Perugia; [b]Università di Perugia, I-6123 Perugia, Italy
[31] University of Oregon, Eugene, OR 97403, USA
[32] Cardiff University, Cardiff CF24 3AA, UK
[33] Syracuse University, Syracuse, NY 13244, USA
[34] Rutherford Appleton Laboratory, HSIC, Chilton, Didcot, Oxon OX11 0QX, UK
[35] [a]IM-PAN 00-956 Warsaw; [b]Warsaw Univ. 00-681; [c]Astro. Obs. Warsaw Univ. 00-478; [d]CAMK-PAM 00-716 Warsaw; [e]Bialystok Univ. 15-424; [f]IPJ 05-400 Swierk-Otwock; [g]Inst. of Astronomy 65-265 Zielona Gora, Poland
[36] University of Maryland, College Park, MD 20742, USA
[37] Laboratoire d'Annecy-le-Vieux de Physique des Particules (LAPP), IN2P3/CNRS, Université de Savoie, F-74941 Annecy-le-Vieux, France
[38] University of Massachusetts-Amherst, Amherst, MA 01003, USA
[39] INFN, [a]Sezione di Firenze, I-50019 Sesto Fiorentino; [b]Università degli Studi di Firenze, I-50121, [c]Firenze; Università degli Studi di Urbino "Carlo Bo," I-61029 Urbino, Italy
[40] NASA/Goddard Space Flight Center, Greenbelt, MD 20771, USA
[41] University of Michigan, Ann Arbor, MI 48109, USA
[42] University of Sannio at Benevento, I-82100 Benevento, Italy
[43] The University of Mississippi, University, MS 38677, USA
[44] Charles Sturt University, Wagga Wagga, NSW 2678, Australia
[45] Caltech-CaRT, Pasadena, CA 91125, USA
[46] INFN, Sezione di Genova, I-16146 Genova, Italy
[47] Carleton College, Northfield, MN 55057, USA
[48] The University of Melbourne, Parkville, VIC 3010, Australia
[49] INFN, [a]Sezione di Roma Tor Vergata; [b]Università di Roma Tor Vergata, [c]Istituto di Fisica dello Spazio Interplanetario (IFSI) INAF, I-00133 Roma; [d]Università dell'Aquila, I-67100 L'Aquila, Italy
[50] Eötvös University, ELTE 1053 Budapest, Hungary
[51] The University of Sheffield, Sheffield S10 2TN, UK
[52] The Pennsylvania State University, University Park, PA 16802, USA
[53] Inter-University Centre for Astronomy and Astrophysics, Pune 411007, India
[54] Southern University and A&M College, Baton Rouge, LA 70813, USA
[55] INFN, [a]Gruppo Collegato di Trento and [b]Università di Trento, I-38050 Povo, Trento, Italy; INFN, [c]Sezione di Padova and [d]Università di Padova, I-35131 Padova, Italy
[56] California Institute of Technology, Pasadena, CA 91125, USA
[57] Laboratoire des Matériaux Avancés (LMA), IN2P3/CNRS, F-69622 Villeurbanne, Lyon, France
[58] University of Rochester, Rochester, NY 14627, USA
[59] The University of Texas at Austin, Austin, TX 78712, USA
[60] Australian National University, Canberra 0200, Australia
[61] Embry-Riddle Aeronautical University, Prescott, AZ 86301, USA
[62] University of Minnesota, Minneapolis, MN 55455, USA
[63] University of Adelaide, Adelaide, SA 5005, Australia
[64] University of Southampton, Southampton SO17 1BJ, UK
[65] Universitat de les Illes Balears, E-07122 Palma de Mallorca, Spain
[66] Northwestern University, Evanston, IL 60208, USA
[67] National Astronomical Observatory of Japan, Tokyo 181-8588, Japan
[68] Institute of Applied Physics, Nizhny Novgorod, 603950, Russia
[69] University of Strathclyde, Glasgow G1 1XQ, UK
[70] Loyola University, New Orleans, LA 70118, USA
[71] Hobart and William Smith Colleges, Geneva, NY 14456, USA
[72] Louisiana Tech University, Ruston, LA 71272, USA
[73] Andrews University, Berrien Springs, MI 49104, USA
[74] Sonoma State University, Rohnert Park, CA 94928, USA
[75] Trinity University, San Antonio, TX 78212, USA
[76] Rochester Institute of Technology, Rochester, NY 14623, USA
[77] Southeastern Louisiana University, Hammond, LA 70402, USA
[78] Department of Physics and Astronomy, University of British Columbia, 6224 Agricultural Road, Vancouver, BC V6T 1Z1, Canada
[79] Département de physique, de génie physique et d'optique, Université Laval, Québec, QC G1K 7P4, Canada
[80] INAF-Osservatorio Astronomico di Cagliari, Poggio dei Pini, 09012 Capoterra, Italy
[81] Dipartimento di Fisica Università di Cagliari, Cittadella Universitaria, I-09042 Monserrato, Italy
[82] Arecibo Observatory, HC 3 Box 53995, Arecibo, PR 00612, USA
[83] West Virginia University, Department of Physics, P.O. Box 6315, Morgantown, WV 26506, USA
[84] Netherlands Institute for Radio Astronomy (ASTRON), Postbus 2, 7990 AA Dwingeloo, The Netherlands
[85] Astronomical Institute "Anton Pannekoek," University of Amsterdam, 1098 SJ Amsterdam, The Netherlands
[86] Australia Telescope National Facility, CSIRO, P.O. Box 76, Epping NSW 1710, Australia
[87] University of Manchester, Jodrell Bank Centre for Astrophysics Alan-Turing Building, Oxford Road, Manchester M13 9PL, UK
[88] Modeling, Algorithms, and Informatics, CCS-3, MS B265, Computer, Computational, and Statistical Sciences Division, Los Alamos National Laboratory, Los Alamos, NM 87545, USA
[89] National Radio Astronomy Observatory, Charlottesville, VA 22903, USA

ABSTRACT

We present a search for gravitational waves from 116 known millisecond and young pulsars using data from the fifth science run of the LIGO detectors. For this search, ephemerides overlapping the run period were obtained for all pulsars using radio and X-ray observations. We demonstrate an updated search method that allows for small

uncertainties in the pulsar phase parameters to be included in the search. We report no signal detection from any of the targets and therefore interpret our results as upper limits on the gravitational wave signal strength. The most interesting limits are those for young pulsars. We present updated limits on gravitational radiation from the Crab pulsar, where the measured limit is now a factor of 7 below the spin-down limit. This limits the power radiated via gravitational waves to be less than $\sim 2\%$ of the available spin-down power. For the X-ray pulsar J0537$-$6910 we reach the spin-down limit under the assumption that any gravitational wave signal from it stays phase locked to the X-ray pulses over timing glitches, and for pulsars J1913+1011 and J1952+3252 we are only a factor of a few above the spin-down limit. Of the recycled millisecond pulsars, several of the measured upper limits are only about an order of magnitude above their spin-down limits. For these our best (lowest) upper limit on gravitational wave amplitude is 2.3×10^{-26} for J1603$-$7202 and our best (lowest) limit on the inferred pulsar ellipticity is 7.0×10^{-8} for J2124$-$3358.

Key words: gravitational waves – pulsars: general

Online-only material: color figures

1. INTRODUCTION

Within our Galaxy, some of the best targets for gravitational wave searches in the sensitive frequency band of current interferometric gravitational wave detectors ($\sim$40–2000 Hz) are millisecond and young pulsars. There are currently just over 200 known pulsars with spin frequencies greater than 20 Hz, which therefore are within this band. In this paper, we describe the latest results from the ongoing search for gravitational waves from these known pulsars using data from the Laser Interferometric Gravitational-Wave Observatory (LIGO). As this search looks for objects with known positions and spin-evolutions, it can use long time spans of data in a fully coherent way to dig deeply into the detector noise. Here we use data from the entire two-year run of the three LIGO detectors, entitled Science Run 5 (S5), during which the detectors reached their design sensitivities (Abbott et al. 2009b). This run started on 2005 November 4 and ended on 2007 October 1. The detectors (the 4 km and 2 km detectors at LIGO Hanford Observatory, H1 and H2, and the 4 km detector at the LIGO Livingston Observatory, L1) had duty factors of 78% for H1, 79% for H2, and 66% for L1. The GEO 600 detector also participated in S5 (Grote & The LIGO Scientific Collaboration 2008), but at lower sensitivities that meant it was not able to enhance this search. The Virgo detector also had data overlapping with S5 during Virgo Science Run 1 (VSR1; Acernese et al. 2008). However, this was also generally at a lower sensitivity than the LIGO detectors and had an observation time of only about four months, meaning that no significant sensitivity improvements could be made by including these data. Due to its multi-stage seismic isolation system Virgo does have better sensitivity than the LIGO detectors below about 40 Hz, opening the possibility of searching for more young pulsars, including the Vela pulsar. These lower frequency searches will be explored more in the future.

This search assumes that the pulsars are triaxial stars emitting gravitational waves at precisely twice their observed spin frequencies, i.e., the emission mechanism is an $\ell = m = 2$ quadrupole, and that gravitational waves are phase-locked with the electromagnetic signal. We use the so-called spin-down limit on strain tensor amplitude h_0^{sd} as a sensitivity target for each pulsar in our analysis. This can be calculated, by assuming that the observed spin-down rate of a pulsar is entirely due to energy loss through gravitational radiation from an $\ell = m = 2$ quadrupole, as

$$h_0^{\mathrm{sd}} = 8.06 \times 10^{-19} I_{38} r_{\mathrm{kpc}}^{-1} (|\dot{\nu}|/\nu)^{1/2}, \tag{1}$$

where I_{38} is the pulsar's principal moment of inertia (I_{zz}) in units of 10^{38} kg m^2, r_{kpc} is the pulsar distance in kpc, ν is the spin-frequency in Hz, and $\dot{\nu}$ is the spin-down rate in Hz s^{-1}. Due to uncertainties in I_{zz} and r, h_0^{sd} is typically uncertain by about a factor of 2. Part of this is due to the uncertainty in I_{zz} which, though predicted to lie roughly in the range 1–3×10^{38} kg m^2, has not been measured for any neutron star; and the best (though still uncertain) prospect is star A of the double pulsar system J0737$-$3039 with 20 years more observation (Kramer & Wex 2009). Distance estimates based on dispersion measure can also be wrong by a factor of 2–3, as confirmed by recent parallax observations of the double pulsar (Deller et al. 2009). For pulsars with measured braking indices, $n = \nu \ddot{\nu}/\dot{\nu}^2$, the assumption that spin-down is dominated by gravitational wave emission is known to be false (the braking index for quadrupolar gravitational wave emission should be 5, but all measured ns are less than 3) and a stricter indirect limit on gravitational wave emission can be set. A phenomenological investigation of some young pulsars (Palomba 2000) indicates that this limit is lower than h_0^{sd} by a factor of 2.5 or more, depending on the pulsar. See Abbott et al. (2007, 2008) for more discussion of the uncertainties in indirect limits. Recycled millisecond pulsars have intrinsically small spin-downs, so for the majority of pulsars in our search these spin-down limits will be well below our current sensitivities, making detection unlikely. However, our search also covers four young pulsars with large spin-down luminosities, and for these we can potentially beat or reach their spin-down limits using current data.

The LIGO band covers the fastest (highest ν) known pulsars, and the quadrupole formula for strain tensor amplitude

$$h_0 = 4.2 \times 10^{-26} \nu_{100}^2 I_{38} \varepsilon_{-6} r_{\mathrm{kpc}}^{-1} \tag{2}$$

indicates that these pulsars are the best gravitational wave emitters for a given equatorial ellipticity $\varepsilon = (I_{xx} - I_{yy})/I_{zz}$ (here $\nu_{100} = \nu/(100\,\mathrm{Hz})$ and $\varepsilon_{-6} = \varepsilon/10^{-6}$). The pulsars with high spin-downs are almost all less than $\sim 10^4$ years old. Usually this is interpreted as greater electromagnetic activity (including particle winds) in younger objects, but it could also mean that they are more active in gravitational wave emission. This is plausible on theoretical grounds too. Strong internal magnetic fields may cause significant ellipticities (Cutler 2002) which would then decay as the field decays or otherwise changes (Goldreich & Reisenegger 1992). The initial crust may be asymmetric if it forms on a timescale on which the neutron star is still perturbed by its violent formation and aftermath, including a possible lengthy perturbation due to the fluid r modes (Lindblom et al. 2000; Wu et al. 2001), and asymmetries may

slowly relax due to mechanisms such as viscoelastic creep. Also the fluid r modes may remain unstable to gravitational wave emission for up to a few thousand years after the neutron star's birth, depending on its composition, viscosity, and initial spin frequency (Owen et al. 1998; Bondarescu et al. 2009). Such r modes are expected to have a gravitational wave frequency about 4/3 the spin frequency. However, we do not report on r-mode searches in this paper.

1.1. Previous Analyses

The first search for gravitational waves from a known pulsar using LIGO and GEO 600 data came from the first science run (S1) in 2002 September. This targeted just one pulsar in the approximately one week worth of data—the then fastest known pulsar J1939+2134 (Abbott et al. 2004). Data from LIGO's second science run (S2), which spanned from 2003 February to 2003 April, were used to search for 28 isolated pulsars (i.e., those not in binary systems; Abbott et al. 2005). The last search for gravitational waves from multiple known pulsars using LIGO data combined data from the third and fourth science runs and had 78 targets, including isolated pulsars and those in binary systems (Abbott et al. 2007). The best (lowest), 95% degree-of-belief, upper limit on gravitational wave amplitude obtained from the search was $h_0^{95\%} = 2.6 \times 10^{-25}$ for J1603−7202, and the best (smallest) limit on ellipticity was just under 10^{-6} for J2124−3358. The data run used in this paper is almost an order of magnitude longer, and has a best strain noise amplitude around a factor of 2 smaller, than that used in the best previous search.

We have also previously searched the first nine months of S5 data for a signal from the Crab pulsar (Abbott et al. 2008). That analysis used two methods to search for a signal: one in which the signal was assumed to be precisely phase-locked with the electromagnetic signal, and another which searched a small range of frequencies and frequency derivatives around the electromagnetic parameters. The time span of data analyzed was dictated by a timing glitch in the pulsar on 2006 August 23, which was used as the end point of the analysis. In that search the spin-down limit for the Crab pulsar was beaten for the first time (indeed it was the first time a spin-down limit had been reached for any pulsar), with a best limit of $h_0^{95\%} = 2.7 \times 10^{-25}$, or slightly below one-fifth of the spin-down limit. This allowed the total power radiated in gravitational waves to be constrained to less than 4% of the spin-down power. We have since discovered an error in the signal template used for the search (Abbott et al. 2009a). We have re-analyzed the data and find a new upper limit based on the early S5 data alone at the higher value shown in Table 3, along with the smaller upper limit based on the full S5 data.

For this analysis, we have approximately 525 days of H1 data, 532 days of H2 data, and 437 days of L1 data. This is using all data flagged as *science mode* during the run (i.e., taken when the detector is locked in its operating condition on the dark fringe of the interference pattern, and relatively stable), except data 1 minute prior to loss of lock, during which time it is often seen to become more noisy.

1.2. Electromagnetic Observations

The radio pulsar parameters used for our searches are based on ongoing radio pulsar monitoring programs, using data from the Jodrell Bank Observatory (JBO), the NRAO 100 m Green Bank Telescope (GBT), and the Parkes radio telescope of the Australia Telescope National Facility. We used radio data coincident with the S5 run as these would reliably represent the pulsars' actual phase evolution during our searches. We obtained data for 44 pulsars from JBO (including the Crab pulsar ephemeris; Lyne et al. 1993, 2009), 39 pulsars within the Terzan 5 and M28 globular clusters from GBT, and 47 from Parkes, including pulsars timed as part of the Parkes Pulsar Timing Array (Manchester 2008). For 15 of these pulsars there were observations from more than one site, making a total of 115 radio pulsars in the analysis (see Table 1 for list of the pulsars, including the observatory and time span of the observations). For the pulsars observed at JBO and Parkes, we have obtained parameters fit to data overlapping with the entire S5 run. For the majority of pulsars observed at GBT, the parameters have been fit to data overlapping approximately the first quarter of S5.

Pulsars generally exhibit timing noise on long timescales. Over tens of years this can cause correlations in the pulse time of arrivals which can give systematic errors in the parameter fits produced, by the standard pulsar timing package TEMPO,[90] of order 2–10 times the regular errors that TEMPO assigns to each parameter (Verbiest et al. 2008), depending on the amplitude of the noise. For our pulsars, with relatively short observation periods of around two years, the long-term timing noise variations should be largely folded in to the parameter fitting, leaving approximately white uncorrelated residuals. Also millisecond pulsars, in general, have intrinsically low levels of timing noise, showing comparatively white residuals. This should mean that the errors produced by TEMPO are approximately the true 1σ errors on the fitted values.

The regular pulse timing observations of the Crab pulsar (Lyne et al. 1993, 2009) indicate that the 2006 August 23 glitch was the only glitch during the S5 run. One other radio pulsar, J1952+3252, was observed to glitch during the run (see Section 5.1.3). Independent ephemerides are available before and after each glitch.

We include one pulsar in our analysis that is not observed as a radio pulsar. This is PSR J0537−6910 in the Large Magellanic Cloud, for which only X-ray timings currently exist. Data for this source come from dedicated time on the *Rossi X-ray Timing Explorer* (*RXTE*; Middleditch et al. 2006) giving ephemerides covering the whole of S5. These ephemerides comprise seven inter-glitch segments, each of which produces phase-stable timing solutions. The segments are separated by times when the pulsar was observed to glitch. Due to the complexity of the pulsar behavior near glitches, which is not reflected in the simple model used to predict pulse times of arrival, sometimes up to ~ 30 days around them are not covered by the ephemerides.

2. GRAVITATIONAL WAVE SEARCH METHOD

The details of the search method are discussed in Dupuis & Woan (2005) and Abbott et al. (2007), but we will briefly review them here. Data from the gravitational wave detectors are heterodyned using twice the known electromagnetic phase evolution of each pulsar, which removes this rapidly varying component of the signal, leaving only the daily varying amplitude modulation caused by each detector's antenna response. Once heterodyned the (now complex) data are low-pass filtered at 0.25 Hz, and then heavily down-sampled, by averaging, from the original sample rate of 16 384 Hz to 1/60 Hz. Using these down-sampled data (B_k, where k represents the kth sample), we

---

[90] http://www.atnf.csiro.au/research/pulsar/tempo/

perform parameter estimation over the signal model $y_k(\boldsymbol{a})$ given the unknown signal parameters $\boldsymbol{a}$. This is done by calculating the posterior probability distribution (Abbott et al. 2007)

$$
p(\boldsymbol{a}|\{B_k\}) \propto \prod_j^M \Bigg(\sum_k^n (\Re\{B_k\} - \Re\{y_k(\boldsymbol{a})\})^2 \\
+ (\Im\{B_k\} - \Im\{y_k(\boldsymbol{a})\})^2 \Bigg)^{-m_j} \times p(\boldsymbol{a}), \quad (3)
$$

where the first term on the right-hand side is the likelihood (marginalized over the data variance, giving a Student's-t-like distribution), $p(\boldsymbol{a})$ is the prior distribution for $\boldsymbol{a}$, M is the number of data segments into which the B_ks have been cut (we assume stationarity of the data during each segment), m_j is the number of data points in the jth segment (with a maximum value of 30, i.e., we only assume stationarity for periods less than, or equal to, 30 minutes in length), and $n = \sum_{j=1}^{j} m_j$. The assumption of Gaussianity and stationarity of the segments holds well for this analysis (see Section 4.5 of Dupuis (2004) for examples of χ^2 and Kolmogorov–Smirnov tests performed to assess these in previous analyses).

We have previously (Abbott et al. 2004, 2005, 2007) performed parameter estimation over the four unknown gravitational wave signal parameters of amplitude h_0, initial phase ϕ_0, cosine of the orientation angle $\cos\iota$, and polarization angle ψ, giving $\boldsymbol{a} = \{h_0, \phi_0, \cos\iota, \psi\}$. Priors on each parameter are set to be uniform over their allowed ranges, with the upper end of the range for h_0 set empirically from the noise level of the data. We choose a uniform prior on h_0 for consistency with our previous analyses (Dupuis & Woan 2005; Abbott et al. 2004, 2005, 2007) and to facilitate straightforward comparison of sensitivity. Extensive trials with software injections have shown this to be a very reasonable choice, returning a conservative (i.e., high) upper limit consistent with the data and any possible signal.

Using a uniformly spaced grid on this four-dimensional parameter space the posterior is calculated at each point. To obtain a posterior for each individual parameter we marginalize over the three others. Using the marginalized posterior on h_0 we can set an upper limit by calculating the value that, integrating up from zero, bounds the required cumulative probability (which we have taken as 95%). We also combine the data from multiple detectors to give a *joint* posterior. To do this, we simply take the product of the likelihoods for each detector and multiply this joint likelihood by the prior. This is possible due to the phase coherence between detectors. Again we can marginalize to produce posteriors for individual parameters.

Below, in Section 2.1, we discuss exploring and expanding this parameter space to more dimensions using a Markov Chain Monte Carlo (MCMC) technique.

2.1. MCMC Parameter Search

When high resolutions are needed it can be computationally time consuming to calculate the posterior over an entire grid as described above, and redundant areas of parameter space with very little probability are explored for a disproportionately large amount of time. A more efficient way to carry out such a search is with an MCMC technique, in which the parameter space is explored more efficiently and without spending much time in the areas with very low probability densities.

An MCMC integration explores the parameter space by stepping from one position in parameter space to another,

comparing the posterior probability of the two points and using a simple algorithm to determine whether the step should be accepted. If accepted it moves to that new position and repeats; if it is rejected it stays at the current position and repeats. Each iteration of the chain, whether it stays in the same position or not, is recorded and the amount of time the chain spends in a particular part of parameter space is directly proportional to the posterior probability density there. The new points are drawn randomly from a specific proposal distribution, often given by a multivariate Gaussian with a mean set as the current position, and a predefined covariance. For an efficient MCMC the proposal distribution should reflect the underlying posterior it is sampling, but any proposal (that does not explicitly exclude the posterior), given enough time, will sample the posterior and deliver an accurate result. We use the Metropolis–Hastings (MH) algorithm to set the acceptance/rejection ratio. Given a current position $\boldsymbol{a}_i$ MH accepts the new position $\boldsymbol{a}_{i+1}$ with probability

$$
\alpha(\boldsymbol{a}_{i+1}|\boldsymbol{a}_i) = \min\left(1, \frac{p(\boldsymbol{a}_{i+1}|d)}{p(\boldsymbol{a}_i|d)}\frac{q(\boldsymbol{a}_i|\boldsymbol{a}_{i+1})}{q(\boldsymbol{a}_{i+1}|\boldsymbol{a}_i)}\right), \quad (4)
$$

where $p(\boldsymbol{a}|d)$ is the posterior value at $\boldsymbol{a}$ given data d and $q(\boldsymbol{a}|\boldsymbol{b})$ is the proposal distribution defining how we choose position $\boldsymbol{a}$ given a current position $\boldsymbol{b}$. In our case we have symmetric proposal distributions, so $q(\boldsymbol{a}_{i+1}|\boldsymbol{a})/q(\boldsymbol{a}_i|\boldsymbol{a}_{i+1}) = 1$ and therefore only the ratio of the posteriors is needed.

A well-tuned MCMC will efficiently explore the parameter space and generate chains that, in histogram form, give the marginalized posterior distribution for each parameter. Defining a good set of proposal distributions for the parameters in $\boldsymbol{a}$ has been done experimentally assuming that they are uncorrelated and therefore have independent distributions. (There are in fact correlations between the h_0 and $\cos\iota$ parameters and the ϕ_0 and ψ parameters, but in our studies these do not significantly alter the efficiency from assuming independent proposals.) The posterior distributions of these parameters will also generally not be Gaussian, especially in low signal-to-noise ratio (S/N) cases (which is the regime in which we expect to be), but a Gaussian proposal is easiest to implement and again does not appear to significantly affect the chain efficiency. We find that, for the angular parameters, Gaussian proposal distributions with standard deviations of an eighth the allowed parameter range (i.e., $\sigma_{\phi_0} = \pi/4$ rad, $\sigma_{\cos\iota} = 1/4$, and $\sigma_\psi = \pi/16$ rad) provide a good exploration of the parameter space (as determined from the ratio of accepted to rejected jumps in the chain) for low S/N signals. We have performed many simulations comparing the output of the MCMC and grid-based searches, both on simulated noise and simulated signals, and both codes give results consistent to within a few percent. In these tests, we find that the computational speed of the MCMC code is about three times faster than the grid-based code, although this can vary by tuning the codes.

An MCMC integration may take time to converge on the bulk of the probability distribution to be sampled, especially if the chains start a long way in parameter space from the majority of the posterior probability. Chains are therefore allowed a *burn-in* phase, during which the positions in the chain are not recorded. For low S/N signals, where the signal amplitude is close to zero and the posteriors are reasonably broad, this burn-in time can be short. To aid the convergence we use simulated annealing in which a temperature parameter is used to flatten the posterior during burn-in to help the chain explore the space more quickly. We do however use techniques to assess whether

our chains have converged (see Brooks & Roberts 1998 for a good overview of convergence assessment tests for MCMCs). We use two such tests: the Geweke test is used on individual chains to compare the means of two independent sections of the chain; and the Gelman and Rubins test is used to compare the variances between and within two or more separate chains. These tests are never absolute indicators of convergence, so each chain also has to be examined manually. The acceptance/rejection ratio of each chain is also looked at as another indicator of convergence. For all our results, discussed in Sections 4 and 5, we have run these tests on the output chains, and conclude that all have converged.

2.2. Adding Phase Parameters

The heterodyne phase is calculated using the parameters measured from electromagnetic observations, which have associated errors. These errors could mean that the heterodyne phase will be offset, and drift away from, the true phase of the signal. Previously we have required that our data be heterodyned with a phase that was known to match the true signal phase over the course of the run to a few degrees. The criterion used to decide on whether to keep, or discard, a pulsar from the analysis was that there was no more than a $30°$ drift of the electromagnetic phase from the signal phase over the course of a data run (Abbott et al. 2007; i.e., if a signal was present the phase drift would lead to a loss in S/N of less than about 15%). In Abbott et al. (2007) this potential phase drift was calculated from the known uncertainties of the heterodyne phase parameters, but without taking into account the covariance between parameters, and as such was an overconservative estimate, risking the possibility that some pulsars were excluded from the analysis unnecessarily.

Rather than just setting an exclusion criterion for pulsars based on the potential phase mismatch (see Section 3) we can instead search over the uncertainties in the phase parameters. This search can also be consistent with the, now provided, covariances on the phase parameters. For pulsars that have small mismatches over the run (that would have been included in the previous analysis), the extra search space allows these small uncertainties to be naturally folded (via marginalization) into the final posteriors on the four main gravitational wave parameters and our eventual upper limit. For pulsars with larger mismatches, which previously would have been excluded, this extra search space allows us to keep them in the analysis and again fold the phase parameter uncertainties into the final result.

We can incorporate the potential phase error into the search by including the phase parameters, as an offset from the heterodyne phase parameters, in the parameter estimation and marginalizing over them. A pulsar with, for example, associated errors on ν, $\dot{\nu}$, right ascension, declination, proper motion in both positional parameters and five orbital binary parameters would add 11 extra parameters to the search. An MCMC is a practical way that allows us to search over these extra parameters. It also means that we make sure we cover enough of the parameter space so as not to miss a signal with a slight phase offset from the heterodyne values. Examples of MCMCs being used in a similar context can be found in Umstätter et al. (2004) and Veitch et al. (2005). However, both these examples attempted to explore far greater parameter ranges than will be applied here. We do not attempt to use the MCMC as a parameter estimation tool for these extra parameters (i.e., due to our expected low S/N regime we would not expect to improve on the given uncertainties of the parameters), but just as a way of making sure we fully cover

the desired parameter space, and fold the uncertainties into our final result without excessive computational cost.

The number of extra parameters included in the search depends on how many parameters were varied to fit the radio data. When fitting parameters with the pulsar timing packages TEMPO, or TEMPO2 (Hobbs et al. 2006), certain values can be held fixed and others left free to vary, so errors will only be given on those allowed to vary. The uncertainties on those parameters that are fit will contain all the overall phase uncertainty.

2.3. Setting up the MCMC

In our search we have information on the likely range over which to explore each parameter as given by the error from the fit (which we take as being the 1σ value of a Gaussian around the best-fit value), and the associated parameter covariance matrix. We use this information to set a prior on these parameters $\boldsymbol{b}$ given by a multivariate Gaussian

$$p(\boldsymbol{b}) \propto \exp\left\{-\frac{1}{2}(\boldsymbol{b}-\boldsymbol{b}_0)^{\mathrm{T}} C^{-1}(\boldsymbol{b}-\boldsymbol{b}_0)\right\}, \qquad (5)$$

with a covariance matrix C. For the vast majority of pulsars, we expect that the uncertainties on the parameters are narrow enough that within their ranges they all give essentially the same phase model (see the discussion of phase mismatch in Section 3). In this case, the posterior on the parameters should be dominated by this prior, therefore a good proposal distribution to efficiently explore the space with is the same multivariate Gaussian.

An example of the posteriors produced when searching over additional parameters (in this case changes in declination and right ascension) can be seen in Figure 1. The figure shows the multivariate Gaussian used as priors on the two parameters and how the posterior is essentially identical to the prior (i.e., the data, which contains no signal, is adding no new information on those parameters, but the full prior space is being explored). We have assessed this technique on many simulations of noise and found that, as expected, the posteriors on the additional phase parameters match the priors. We have also tested this technique on many software simulated signals (using real pulsar phase parameters) by offsetting the injected signal parameters from the "best-fit" values by amounts consistent with the parameter covariance matrix. In these tests, we have been able to extract the parameters as expected.

2.4. Hardware Injections

During all LIGO science runs, except the first, fake pulsar signals have been injected into the detectors by direct actuation of the end test masses. These have provided end-to-end validation of the analysis codes with coherence between the different detectors. During S5, as with S3 and S4 (Abbott et al. 2007), 10 signals with different source parameters were injected into the detectors. As a demonstration of the analysis method these have been extracted using the MCMC (over the four main parameters only) and all have been recovered with their known injection parameter values. The extracted parameters for the two strongest signals are shown in Figure 2. From these injections it can be seen that the parameters can be extracted to a high accuracy and consistently between detectors. The offsets in the extracted values from the injected values are within a few percent. These are well within the expected uncertainties of the detector calibration, which are approximately 10%, 10%, and 13% in amplitude, and $4°\!.3$ (0.08 rad), $3°\!.4$ (0.06 rad), and $2°\!.3$ (0.04 rad) in phase for H1, H2, and L1, respectively.
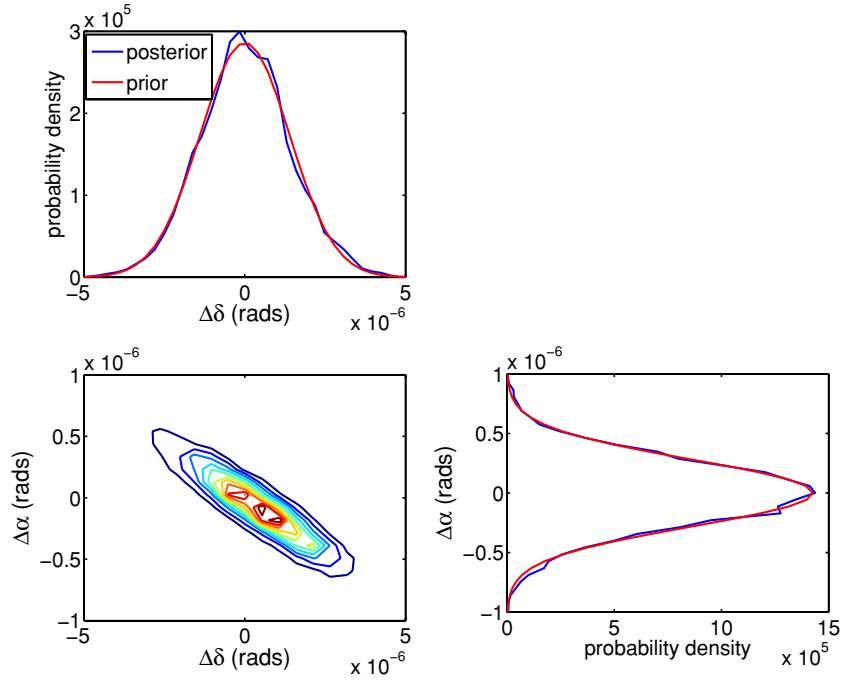
Figure 1. Posteriors and priors on offsets in declination δ and right ascension α computed from an MCMC search for PSR J0407+1607 using a day of simulated data containing no signal. The covariance contour plot of the MCMC chains for the two parameters is shown and has a correlation coefficient of -0.93, which is identical to that of the multivariate Gaussian prior distribution used in this study.

(A color version of this figure is available in the online journal.)
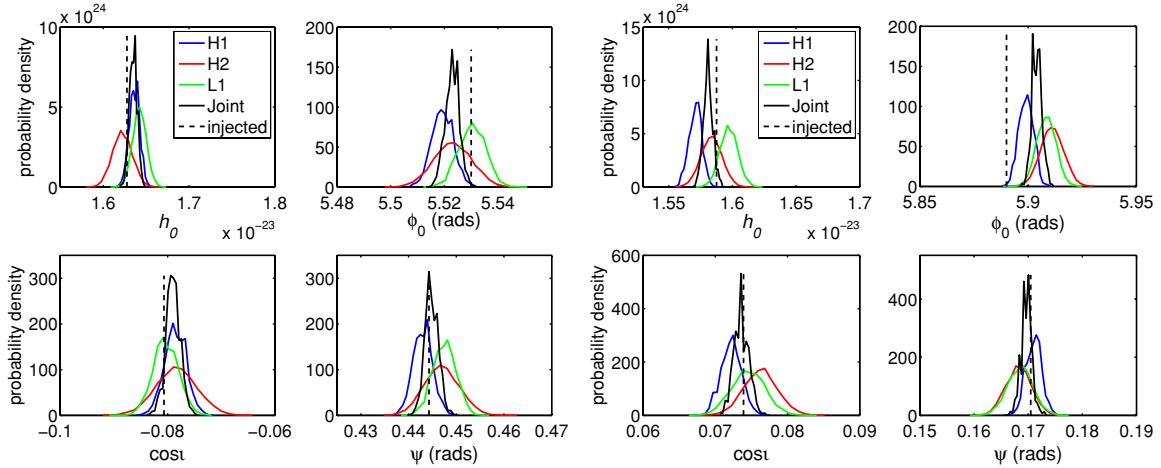
Figure 2. Extracted posteriors for the pulsar parameters from the two strongest hardware injections for each detector and for a joint detector analysis. In each plot the injected parameter value is marked by a dashed vertical line. The left pulsar injection was at a frequency of 108.9 Hz and the right pulsar was at 194.3 Hz.

(A color version of this figure is available in the online journal.)

3. EVALUATION OF PULSAR PARAMETER ERRORS

For the majority of pulsars we have parameter correlation matrices that have been produced during the fit to the radio data, and (as discussed in Section 2.2) we can use these to search over the uncertainties on the phase parameters. For some pulsars no correlation matrix was produced with the radio observations, so for these we instead construct conservative correlation matrices. These assume no correlations between any parameters, except in the case of binary systems for which we assume a correlation of 1 between the angle and time of periastron. This gives a slightly conservative overestimate of the parameter errors, but is still a useful approximation for our purposes. From these correlation matrices and the given parameter standard deviations we produce a covariance matrix for each pulsar.

Using these covariance matrices we can also assess the potential phase mismatch that might occur between the true signal and the best-fit signal used in the heterodyne due to errors in the pulsar phase parameters (as discussed in Section 2.2.) We take the mismatch (i.e., the loss in signal power caused by the heterodyne phase being offset, over time, from the true signal phase) to be

$$M = 1 - \left(\frac{1}{T} \int_0^T \cos\left\{\phi(\boldsymbol{b} + \delta\boldsymbol{b}, t) - \phi(\boldsymbol{b}, t)\right\} dt \right)^2, \quad (6)$$

where ϕ is the phase given a vector of phase parameters $\boldsymbol{b}$ at time t and T is the total observation time. To get offsets in the phase parameters, $\delta\boldsymbol{b}$, we draw random values from the

multivariate Gaussian defined by the covariance matrix. For each pulsar, we drew 100,000 random points and calculated the mean and maximum mismatch over the period of the S5 run. The mean mismatch is a good indicator of whether the given best-fit parameter values are adequate for our search, or whether the potential offset is large and a search including the phase parameters is entirely necessary. The maximum mismatch represents a potential worst case in which the true signal parameters are at a point in parameter space approximately 4.5σ from the best-fit values (the maximum mismatch will obviously increase if one increases the number of randomly drawn values). Of our 113 non-glitching pulsars there are only 16 pulsars with *mean* mismatches greater than 1%, three of which are greater than 10%: J0218+4232 at $\sim$43%, J0024$-$7204H at $\sim$15%, and J1913+1011 at $\sim$37%. Given the exclusion criterion for the S3 and S4 analyses (see Section 2.2), these three pulsars would have been removed from this analysis. There are 16 pulsars with *maximum* mismatches greater than 10% with three of these being at almost 100%—i.e., if the signal parameters truly were offset from their best-fit values by this much, and these parameters were not searched over, then the signal would be completely missed. This suggests that for the majority of pulsars the search over the four main parameters of h_0, ϕ_0, $\cos\iota$, and ψ is all that is necessary. But for a few, and in particular the three with large mean mismatches (J0218+4232, J0024$-$7204H, and J1913+1011), the search over the extra parameters is needed to ensure not losing signal power.

4. ANALYSIS

We have used the MCMC search over *all* phase parameters, where they have given errors, for all but three pulsars (see below). For the majority of pulsars it is unnecessary (though harmless) to include these extra parameters in the search as their priors are so narrow, but it does provide an extra demonstration of the flexibility of the method. To double check, we also produced results for each pulsar using the four dimensional grid of the earlier analyses and found that, for pulsars with negligible mismatch, the results were consistent to within a few percent.

For our full analysis we produced three independent MCMC chains with burn-in periods of 100,000 iterations, followed by 100,000 iterations to sample the posterior. The three chains were used to assess convergence using the tests discussed above in Section 2.1. All chains were seen to converge and were therefore combined to give a total chain length of 300,000 iterations from which the posteriors were generated.

For the three pulsars that glitched during S5 (the Crab, J1952+3252, and J0539$-$6910), the MCMC was not used to search over the position and frequency parameters as above, as the uncertainties on these parameters gave negligible potential mismatch. Our analysis of these pulsars did however include extra parameters in the MCMC to take into account potential uncertainties in the model caused by the glitches. We analyzed the data coherently over the full run as well as in stretches separated by the glitches that are treated separately. We also included a model that allowed for a fixed but unknown phase jump $\Delta\phi$ at the time of each glitch, keeping other physical parameters fixed across the glitch. Results for all of these cases are given in Section 5.1.

The maximum detector calibration uncertainties are approximately 10%, 10%, and 13% in amplitude, and $4°.3$ (0.08 rad), $3°.4$ (0.06 rad), and $2°.3$ (0.04 rad) in phase for H1, H2, and L1, respectively.

5. RESULTS

No evidence of a gravitational wave signal was seen for any of the pulsars. In light of this, we present joint 95% upper limits on h_0 for each pulsar (see Table 1 for the results for the non-glitching pulsars). We also interpret these as limits on the pulsar ellipticity, given by

$$\varepsilon = 0.237\,h_{-24}r_{\mathrm{kpc}}\nu^{-2}I_{38}, \qquad (7)$$

where h_{-24} is the h_0 upper limit in units of 1×10^{-24}, $I_{38} = 1$, and r_{kpc} is the pulsar distance in kpc. For the majority of pulsars, this distance is taken as the estimate value from Australia Telescope National Facility Pulsar Catalogue[91] (Manchester et al. 2005), but for others more up-to-date distances are known. For pulsars in Terzan 5 (those with the name J1748$-$2446), a distance of 5.5 kpc is used (Ortolani et al. 2007). For J1939+2134 the best estimate distance is a highly uncertain value of $\sim8.3\pm5$ kpc based on parallax measurements (Kaspi et al. 1994), but it is thought to be a large overestimate, so instead we use a value of 3.55 kpc derived from the Cordes & Lazio (2002) NE2001 galactic electron density model. The observed spin-down rate for globular cluster pulsars is contaminated by the accelerations within the cluster, which can lead to some seeming to spin-up as can be seen in column four of Table 1. For all pulsars in globular clusters, except J1824$-$2452A, we instead calculate a conservative spin-down limit by assuming all pulsars have a characteristic age $\tau = \nu/2\dot\nu$ of 10^9 years. Note that using the characteristic age gives a spin-down limit that is independent of frequency and only depends on τ and r. Globular cluster pulsar J1824$-$2452A has a large spin-down that is well above what could be masked by cluster accelerations. Therefore, for this pulsar we use its true spin-down for our limit calculation. For some nearby pulsars there is a small, but measurable, Shklovskii effect which will contaminate the observed spin-down. For these if a value of the intrinsic spin-down is known then this is used when calculating the spin-down limit.

The results are plotted in histogram form in Figure 3. Also shown for comparison are the results of the previous search using combined data from the S3 and S4 science runs. The median upper limit on h_0 for this search, at 7.2×10^{-26}, is about an order of magnitude better than in the previous analysis (6.3×10^{-25}). A large part of this increased sensitivity (about a factor of 4–5) is due the longer observation time. The median ellipticity is $\varepsilon = 1.1\times10^{-6}$, an improvement from 9.1×10^{-6}, and the median ratio to the spin-down limit is 108, improved from 870. If one excludes the conservatively estimated spin-down limits for the globular cluster pulsars, the median ratio is 73. In Figure 4, the upper limits on h_0 are also plotted overlaid onto an estimate of the search sensitivity.[92] The expected uncertainties in these results due to the calibrations are given in Section 2.4.

The smallest upper limit on h_0 for any pulsar is 2.3×10^{-26} for J1603$-$7202, which has a gravitational wave frequency of 135 Hz and is in the most sensitive part of the detectors' bands. The lowest ellipticity upper limit is 7.0×10^{-8} for J2124$-$3358,

---

[91] http://www.atnf.csiro.au/research/pulsar/psrcat/
[92] The upper and lower estimated sensitivity limits for the shaded band in Figure 4 come from the values of the 95% h_0 upper limits that bound 95% of total values from simulations on white noise for randomly distributed pulsars. The band can be estimated from Figure 1 of Dupuis & Woan (2005), which gives limits of $(7$–$20)\times\sqrt{S_n/T}$, where S_n is the single-sided power spectral density and T is the total observation time in seconds.

ABBOTT ET AL.

Table 1
Information on the Non-glitching Pulsars in Our Search, Including the Start and End Times of the Radio Observations Used in Producing the Parameter Fits for Our Search, and Upper Limit Results

Pulsar	Start–End (MJD)	ν (Hz)	$\dot{\nu}$ (Hz s^{-1})	Distance (kpc)	Spin-down Limit	Joint $h_0^{95\%}$	Ellipticity	$h_0^{95\%}/h_0^{\rm sd}$
J0024$-$7204C[cp]	48383–54261	173.71	1.5×10^{-15}	4.9	6.55×10^{-28}	5.88×10^{-25}	2.26×10^{-5}	898
J0024$-$7204D[cp]	48465–54261	186.65	1.2×10^{-16}	4.9	6.55×10^{-28}	4.45×10^{-26}	1.48×10^{-6}	68
J0024$-$7204E[bcp]	48465–54261	282.78	-7.9×10^{-15}	4.9	6.55×10^{-28}	9.97×10^{-26}	1.44×10^{-6}	152
J0024$-$7204F[cp]	48465–54261	381.16	-9.4×10^{-15}	4.9	6.55×10^{-28}	8.76×10^{-26}	6.98×10^{-7}	134
J0024$-$7204G[cp]	48600–54261	247.50	2.6×10^{-15}	4.9	6.55×10^{-28}	1.00×10^{-25}	1.90×10^{-6}	153
J0024$-$7204H[bcp]	48518–54261	311.49	1.8×10^{-16}	4.9	6.55×10^{-28}	6.44×10^{-26}	7.69×10^{-7}	98
J0024$-$7204I[bcp]	50684–54261	286.94	3.8×10^{-15}	4.9	6.55×10^{-28}	5.19×10^{-26}	7.30×10^{-7}	79
J0024$-$7204J[bcp]	48383–54261	476.05	2.2×10^{-15}	4.9	6.55×10^{-28}	1.04×10^{-25}	5.34×10^{-7}	159
J0024$-$7204L[cp]	50687–54261	230.09	6.5×10^{-15}	4.9	6.55×10^{-28}	5.82×10^{-26}	1.27×10^{-6}	89
J0024$-$7204M[cp]	48495–54261	271.99	2.8×10^{-15}	4.9	6.55×10^{-28}	6.14×10^{-26}	9.61×10^{-7}	94
J0024$-$7204N[cp]	48516–54261	327.44	2.4×10^{-15}	4.9	6.55×10^{-28}	8.35×10^{-26}	9.02×10^{-7}	128
J0024$-$7204Q[bcp]	50690–54261	247.94	-2.1×10^{-15}	4.9	6.55×10^{-28}	5.74×10^{-26}	1.08×10^{-6}	88
J0024$-$7204R[bcp]	50743–54261	287.32	-1.2×10^{-14}	4.9	6.55×10^{-28}	5.53×10^{-26}	7.76×10^{-7}	84
J0024$-$7204S[bcp]	50687–54241	353.31	1.5×10^{-14}	4.9	6.55×10^{-28}	6.82×10^{-26}	6.33×10^{-7}	104
J0024$-$7204T[bcp]	50684–54261	131.78	-5.1×10^{-15}	4.9	6.55×10^{-28}	3.34×10^{-26}	2.23×10^{-6}	51
J0024$-$7204U[bcp]	48516–54261	230.26	-5.0×10^{-15}	4.9	6.55×10^{-28}	5.63×10^{-26}	1.23×10^{-6}	86
J0024$-$7204Y[bcp]	51504–54261	455.24	7.3×10^{-15}	4.9	6.55×10^{-28}	9.42×10^{-26}	5.26×10^{-7}	144
J0218+4232[bj]	49092–54520	430.46	-1.4×10^{-14a}	5.8	7.91×10^{-28}	1.47×10^{-25}	1.10×10^{-6}	186
J0407+1607[bj]	52719–54512	38.91	-1.2×10^{-16}	4.1	3.48×10^{-28}	6.18×10^{-26}	3.93×10^{-5}	178
J0437$-$4715[bp]	53683–54388	173.69	-4.7×10^{-16a}	0.1	8.82×10^{-27}	5.73×10^{-25}	6.74×10^{-7}	65
J0613$-$0200[bjp]	53406–54520	326.60	-9.8×10^{-16a}	0.5	2.91×10^{-27}	1.11×10^{-25}	1.18×10^{-7}	38
J0621+1002[bj]	52571–54516	34.66	-5.5×10^{-17a}	1.9	5.40×10^{-28}	1.53×10^{-25}	5.65×10^{-5}	284
J0711$-$6830[p]	53687–54388	182.12	-2.7×10^{-16a}	1.0	9.52×10^{-28}	5.00×10^{-26}	3.71×10^{-7}	53
J0737$-$3039A[bj]	53595–54515	44.05	-3.4×10^{-15a}	1.1	6.17×10^{-27}	7.87×10^{-26}	1.10×10^{-5}	13
J0751+1807[bj]	53405–54529	287.46	-6.3×10^{-16a}	0.6	1.92×10^{-27}	1.64×10^{-25}	2.91×10^{-7}	85
J1012+5307[bj]	53403–54523	190.27	-4.7×10^{-16a}	0.5	2.43×10^{-27}	6.94×10^{-26}	2.36×10^{-7}	29
J1022+1001[bjp]	53403–54521	60.78	-1.6×10^{-16}	0.4	3.27×10^{-27}	4.44×10^{-26}	1.14×10^{-6}	14
J1024$-$0719[jp]	53403–54501	193.72	-6.9×10^{-16}	0.5	2.88×10^{-27}	5.01×10^{-26}	1.67×10^{-7}	17
J1045$-$4509[bp]	53688–54386	133.79	-2.0×10^{-16a}	3.2	3.00×10^{-28}	4.37×10^{-26}	1.87×10^{-6}	145
J1455$-$3330[bj]	52688–54524	125.20	-2.5×10^{-16a}	0.7	1.53×10^{-27}	5.15×10^{-26}	5.75×10^{-7}	34
J1600$-$3053[bp]	53688–54386	277.94	-6.5×10^{-16a}	2.7	4.62×10^{-28}	5.57×10^{-26}	4.55×10^{-7}	121
J1603$-$7202[bp]	53688–54385	67.38	-5.9×10^{-17a}	1.6	4.62×10^{-28}	2.32×10^{-26}	1.98×10^{-6}	50
J1623$-$2631[bcj]	53403–54517	90.29	-5.5×10^{-15}	2.2	1.46×10^{-27}	5.81×10^{-26}	3.71×10^{-6}	40
J1640+2224[bj]	53410–54506	316.12	-1.6×10^{-16a}	1.2	4.86×10^{-28}	6.65×10^{-26}	1.87×10^{-7}	137
J1643$-$1224[bjp]	52570–54517	216.37	-6.8×10^{-16a}	4.9	2.94×10^{-28}	4.35×10^{-26}	1.07×10^{-6}	148
J1701$-$3006A[bcp]	53590–54391	190.78	4.8×10^{-15}	6.9	4.65×10^{-28}	5.82×10^{-26}	2.61×10^{-6}	125
J1701$-$3006B[bcp]	53650–54391	278.25	2.7×10^{-14}	6.9	4.65×10^{-28}	7.63×10^{-26}	1.61×10^{-6}	164
J1701$-$3006C[bcp]	53590–54396	131.36	1.1×10^{-15}	6.9	4.65×10^{-28}	3.52×10^{-26}	3.32×10^{-6}	76
J1713+0747[bjp]	53406–54509	218.81	-3.8×10^{-16a}	1.1	9.54×10^{-28}	4.44×10^{-26}	2.45×10^{-7}	47
J1730$-$2304[jp]	52571–54519	123.11	-3.1×10^{-16}	0.5	2.49×10^{-27}	5.93×10^{-26}	4.72×10^{-7}	24
J1732$-$5049[bp]	53725–54386	188.23	-4.9×10^{-16}	1.8	7.18×10^{-28}	5.25×10^{-26}	6.34×10^{-7}	73
J1744$-$1134[jp]	52604–54519	245.43	-4.1×10^{-16a}	0.5	2.18×10^{-27}	1.10×10^{-25}	2.07×10^{-7}	50
J1748$-$2446A[bcjg]	52320–54453	86.48	2.2×10^{-16}	5.5	5.83×10^{-28}	3.89×10^{-26}	6.77×10^{-6}	67
J1748$-$2446C[cjg]	53403–54516	118.54	8.5×10^{-15}	5.5	5.83×10^{-28}	5.00×10^{-26}	4.63×10^{-6}	86
J1748$-$2446D[cg]	50851–53820	212.13	-5.7×10^{-15}	5.5	5.83×10^{-28}	6.78×10^{-26}	1.96×10^{-6}	116
J1748$-$2446E[bcg]	53193–53820	455.00	3.8×10^{-15}	5.5	5.83×10^{-28}	8.95×10^{-26}	5.62×10^{-7}	153
J1748$-$2446F[cg]	53193–53820	180.50	-1.3×10^{-16}	5.5	5.83×10^{-28}	8.37×10^{-26}	3.34×10^{-6}	143
J1748$-$2446G[cg]	51884–53820	46.14	-8.4×10^{-16}	5.5	5.83×10^{-28}	5.82×10^{-26}	3.56×10^{-5}	100
J1748$-$2446H[cg]	51884–53820	203.01	3.4×10^{-15}	5.5	5.83×10^{-28}	7.81×10^{-26}	2.46×10^{-6}	134
J1748$-$2446I[bcg]	50851–54195	104.49	7.3×10^{-16}	5.5	5.83×10^{-28}	3.54×10^{-26}	4.21×10^{-6}	61
J1748$-$2446K[cg]	51884–53820	336.74	1.1×10^{-14}	5.5	5.83×10^{-28}	6.67×10^{-26}	7.65×10^{-7}	114
J1748$-$2446L[cg]	51884–53820	445.49	3.4×10^{-15}	5.5	5.83×10^{-28}	1.39×10^{-25}	9.09×10^{-7}	238
J1748$-$2446M[bcg]	51884–53820	280.15	-3.9×10^{-14}	5.5	5.83×10^{-28}	1.01×10^{-25}	1.68×10^{-6}	173
J1748$-$2446N[bcg]	53193–54195	115.38	-7.4×10^{-15}	5.5	5.83×10^{-28}	5.85×10^{-26}	5.71×10^{-6}	100
J1748$-$2446O[bcg]	52500–53957	596.43	2.5×10^{-14}	5.5	5.83×10^{-28}	2.65×10^{-25}	9.68×10^{-7}	454
J1748$-$2446P[bcg]	53193–54557	578.50	-8.7×10^{-14}	5.5	5.83×10^{-28}	1.56×10^{-25}	6.08×10^{-7}	267
J1748$-$2446Q[bcg]	53193–54139	355.62	4.6×10^{-15}	5.5	5.83×10^{-28}	8.80×10^{-26}	9.05×10^{-7}	151
J1748$-$2446R[cg]	52500–53820	198.86	-1.9×10^{-14}	5.5	5.83×10^{-28}	8.23×10^{-26}	2.71×10^{-6}	141
J1748$-$2446S[cg]	53193–53820	163.49	-1.7×10^{-15}	5.5	5.83×10^{-28}	4.46×10^{-26}	2.17×10^{-6}	76
J1748$-$2446T[cg]	51884–53819	141.15	-6.1×10^{-15}	5.5	5.83×10^{-28}	5.12×10^{-26}	3.34×10^{-6}	88
J1748$-$2446V[bcg]	53193–53820	482.51	2.2×10^{-14}	5.5	5.83×10^{-28}	1.26×10^{-25}	7.04×10^{-7}	216
J1748$-$2446W[bcg]	52500–53820	237.80	-7.1×10^{-15}	5.5	5.83×10^{-28}	9.57×10^{-26}	2.20×10^{-6}	164
J1748$-$2446X[bcg]	51884–54139	333.44	-6.5×10^{-15}	5.5	5.83×10^{-28}	8.18×10^{-26}	9.57×10^{-7}	140
J1748$-$2446Y[bcg]	53193–53820	488.24	-4.0×10^{-14}	5.5	5.83×10^{-28}	2.10×10^{-25}	1.15×10^{-6}	360
J1748$-$2446Z[bcg]	53193–54139	406.08	1.4×10^{-14}	5.5	5.83×10^{-28}	8.43×10^{-26}	6.65×10^{-7}	145

Table 1
(Continued)

Pulsar	Start–End (MJD)	ν (Hz)	$\dot{\nu}$ (Hz s^{-1})	Distance (kpc)	Spin-down Limit	Joint $h_0^{95\%}$	Ellipticity	$h_0^{95\%}/h_0^{sd}$
J1748−2446aa[cg]	51884–53819	172.77	1.3×10^{-14}	5.5	5.83×10^{-28}	2.28×10^{-25}	9.92×10^{-6}	391
J1748−2446ab[cg]	51884–53819	195.32	-1.6×10^{-14}	5.5	5.83×10^{-28}	4.67×10^{-26}	1.59×10^{-6}	80
J1748−2446ac[cg]	52500–53819	196.58	-8.8×10^{-15}	5.5	5.83×10^{-28}	7.19×10^{-26}	2.42×10^{-6}	123
J1748−2446ad[bcg]	53204–54557	716.36	1.7×10^{-14}	5.5	5.83×10^{-28}	1.77×10^{-25}	4.48×10^{-7}	303
J1748−2446ae[bcg]	53193–53820	273.33	4.3×10^{-14}	5.5	5.83×10^{-28}	6.57×10^{-26}	1.14×10^{-6}	113
J1748−2446af[cg]	53193–53820	302.63	2.1×10^{-14}	5.5	5.83×10^{-28}	1.07×10^{-25}	1.52×10^{-6}	183
J1748−2446ag[cg]	53193–53819	224.82	-6.3×10^{-16}	5.5	5.83×10^{-28}	9.49×10^{-26}	2.44×10^{-6}	163
J1748−2446ah[cg]	53193–53819	201.40	-2.3×10^{-14}	5.5	5.83×10^{-28}	5.49×10^{-26}	1.76×10^{-6}	94
J1756−2251[bj]	53403–54530	35.14	-1.3×10^{-15}	2.9	1.65×10^{-27}	9.70×10^{-26}	5.42×10^{-5}	59
J1801−1417[j]	53405–54505	275.85	-4.0×10^{-16}	1.8	5.42×10^{-28}	6.15×10^{-26}	3.44×10^{-7}	113
J1803−30[cp]	53654–54379	140.83	-1.0×10^{-15}	7.8	4.11×10^{-28}	5.51×10^{-26}	5.12×10^{-6}	134
J1804−0735[bcj]	52573–54518	43.29	-8.8×10^{-16}	8.4	3.82×10^{-28}	8.44×10^{-26}	8.95×10^{-5}	221
J1804−2717[bj]	52574–54453	107.03	-4.7×10^{-16}	1.2	1.44×10^{-27}	2.40×10^{-26}	5.79×10^{-7}	17
J1807−2459A[bcp]	53621–54462	326.86	4.8×10^{-16}	2.7	1.19×10^{-27}	1.53×10^{-25}	9.13×10^{-7}	129
J1810−2005[bj]	53406–54508	30.47	-1.4×10^{-16}	4.0	4.28×10^{-28}	2.22×10^{-25}	2.28×10^{-4}	519
J1823−3021A[cj]	53403–54530	183.82	-1.1×10^{-13}	7.9	4.06×10^{-28}	3.93×10^{-26}	2.17×10^{-6}	97
J1824−2452A[cjpg]	53403–54509	327.41	-1.7×10^{-13}	4.9	3.79×10^{-27}	7.80×10^{-26}	8.43×10^{-7}	21
J1824−2452B[cg]	53629–54201	152.75	5.6×10^{-15}	4.9	6.55×10^{-28}	4.26×10^{-26}	2.11×10^{-6}	65
J1824−2452C[bcg]	52335–54202	240.48	-9.8×10^{-15}	4.9	6.55×10^{-28}	6.48×10^{-26}	1.30×10^{-6}	99
J1824−2452E[cg]	53629–54201	184.53	3.7×10^{-15}	4.9	6.55×10^{-28}	7.51×10^{-26}	2.55×10^{-6}	115
J1824−2452F[cg]	52497–54114	407.97	-1.6×10^{-15}	4.9	6.55×10^{-28}	9.74×10^{-26}	6.78×10^{-7}	149
J1824−2452G[bcg]	53629–54202	169.23	-5.2×10^{-15}	4.9	6.55×10^{-28}	7.23×10^{-26}	2.93×10^{-6}	110
J1824−2452H[bcg]	53629–54202	216.01	-3.6×10^{-15}	4.9	6.55×10^{-28}	8.27×10^{-26}	2.05×10^{-6}	126
J1824−2452J[bcg]	53629–54201	247.54	4.7×10^{-15}	4.9	6.55×10^{-28}	1.07×10^{-25}	2.03×10^{-6}	163
J1841+0130[bj]	53405–54513	33.59	-9.2×10^{-15}	3.2	4.19×10^{-27}	1.65×10^{-25}	1.10×10^{-4}	39
J1843−1113[j]	53353–54508	541.81	-2.8×10^{-15}	2.0	9.33×10^{-28}	1.64×10^{-25}	2.61×10^{-7}	176
J1857+0943[bjp]	53409–54517	186.49	-6.0×10^{-16a}	0.9	1.59×10^{-27}	7.27×10^{-26}	4.50×10^{-7}	46
J1905+0400[j]	53407–54512	264.24	-3.4×10^{-16}	1.3	6.81×10^{-28}	7.40×10^{-26}	3.36×10^{-7}	109
J1909−3744[bp]	53687–54388	339.32	-3.1×10^{-16a}	1.1	6.78×10^{-28}	8.09×10^{-26}	1.89×10^{-7}	119
J1910−5959A[bcp]	53666–54380	306.17	-2.8×10^{-16}	4.5	7.13×10^{-28}	7.71×10^{-26}	8.75×10^{-7}	108
J1910−5959B[cp]	53609–54473	119.65	1.1×10^{-14}	4.5	7.13×10^{-28}	3.81×10^{-26}	2.83×10^{-6}	53
J1910−5959C[cp]	53666–54390	189.49	-7.8×10^{-17}	4.5	7.13×10^{-28}	4.34×10^{-26}	1.29×10^{-6}	61
J1910−5959D[cp]	53621–54460	110.68	-1.2×10^{-14}	4.5	7.13×10^{-28}	3.03×10^{-26}	2.63×10^{-6}	42
J1910−5959E[cp]	53610–54441	218.73	2.1×10^{-14}	4.5	7.13×10^{-28}	4.77×10^{-26}	1.06×10^{-6}	67
J1911+1347[j]	53403–54530	216.17	-8.0×10^{-16}	1.6	9.63×10^{-28}	7.00×10^{-26}	5.70×10^{-7}	73
J1911−1114[bj]	53407–54512	275.81	-4.8×10^{-16a}	1.6	6.66×10^{-28}	5.62×10^{-26}	2.78×10^{-7}	84
J1913+1011[j]	53745–54911	27.85	-2.6×10^{-12}	4.5	5.51×10^{-26}	2.14×10^{-25}	2.93×10^{-4}	3.9
J1939+2134[jp]	53407–54519	641.93	-4.3×10^{-14a}	3.5	1.86×10^{-27}	1.79×10^{-25}	3.65×10^{-7}	96
J1955+2908[bj]	53403–54524	163.05	-7.6×10^{-16a}	5.4	3.23×10^{-28}	7.07×10^{-26}	3.39×10^{-6}	219
J2019+2425[bj]	53599–54505	254.16	-1.7×10^{-16a}	0.9	7.14×10^{-28}	9.23×10^{-26}	3.07×10^{-7}	129
J2033+17[bj]	53702–54522	168.10	-3.1×10^{-16}	1.4	7.93×10^{-28}	7.49×10^{-26}	8.65×10^{-7}	94
J2051−0827[bj]	53410–54520	221.80	-6.1×10^{-16a}	1.3	1.04×10^{-27}	7.57×10^{-26}	4.65×10^{-7}	73
J2124−3358[jp]	53410–54510	202.79	-5.1×10^{-16a}	0.2	5.13×10^{-27}	4.85×10^{-26}	6.96×10^{-8}	9.4
J2129−5721[bp]	53687–54388	268.36	-2.0×10^{-15a}	2.5	8.71×10^{-28}	6.12×10^{-26}	5.13×10^{-7}	70
J2145−0750[bjp]	53409–54510	62.30	-1.0×10^{-16a}	0.5	2.05×10^{-27}	3.83×10^{-26}	1.17×10^{-6}	19
J2229+2643[bj]	53403–54524	335.82	-1.6×10^{-16}	1.4	3.95×10^{-28}	9.89×10^{-26}	2.96×10^{-7}	250
J2317+1439[bj]	53406–54520	290.25	-1.3×10^{-16a}	1.9	2.82×10^{-28}	8.83×10^{-26}	4.68×10^{-7}	313
J2322+2057[j]	53404–54519	207.97	-1.8×10^{-16a}	0.8	9.55×10^{-28}	1.12×10^{-25}	4.78×10^{-7}	117

Notes.

[a] The pulsar's spin-down is corrected for proper motion effects.

[b] The pulsar is within a binary system.

[c] The pulsar is within a globular cluster.

[g] The pulsar was observed by the GBT.

[j] The pulsar was observed by the JBO.

[p] The pulsar was observed by the Parkes Observatory.

which has a gravitational wave frequency of 406 Hz and a best estimate distance of 0.2 kpc. Of the millisecond recycled pulsars this is also the closest to its spin-down limit, at a value of 9.4 times greater than this limit. Of all pulsars which did not glitch during S5, the young pulsar J1913+1011 is the closest to its spin-down limit, at only 3.9 times greater than it.

5.1. Glitching Pulsars

For the three pulsars that glitched, we have chosen to take into account three different models related to the coherence of the gravitational wave signal and the electromagnetic signal over the glitch: (1) there is coherence between them over the glitch (i.e., the glitch causes no discontinuity between the electromagnetic
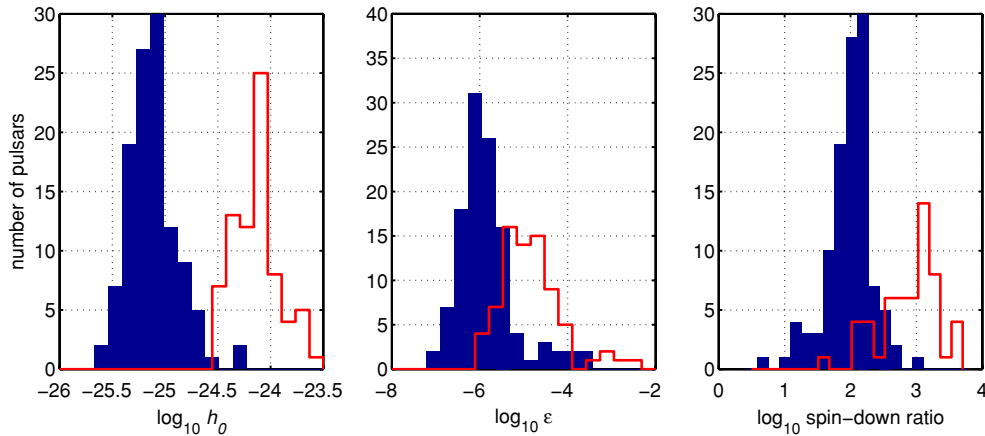
Figure 3. Solid histograms show the results of this analysis in terms of upper limits on h_0, the ellipticity ε, and the ratio to the spin-down limit (excluding the glitching pulsars). The clear histograms show the same set of values for the combined S3 and S4 analysis (Abbott et al. 2007).

(A color version of this figure is available in the online journal.)

and gravitational wave phases); (2) there is decoherence (in terms of a phase jump) between them at the time of the glitch, but the phase discontinuity is included as an extra search parameter (i.e., a $\Delta\phi$ parameter is added at the time of the glitch); and (3) the data stretch before, between, and after the glitches are treated separately and analyzed independently.

5.1.1. Crab Pulsar

For this search, we include the three different models described above relating to the observed glitch in the pulsar on 2006 August 3. Potentially all the four main gravitational wave signal parameters could be changed during the glitch if it is large enough to cause major disruption to the star, but this is not the case for the observed glitch. It had a fractional frequency change of order $\Delta\nu/\nu \sim 5 \times 10^{-9}$, which is unlikely to be energetic enough to cause changes in the gravitational wave amplitude near our current levels of sensitivity. To model the signal phase, we use the regularly updated Crab pulsar Monthly Ephemeris (Lyne et al. 1993, 2009), which is needed to take into account the phase variations caused by timing noise.

As for the previous Crab pulsar search (Abbott et al. 2008), we have information on the orientation of the pulsar from the orientation of the pulsar wind nebula (PWN; Ng & Romani 2008). We use this information to set Gaussian priors on the ψ and ι parameters of $\psi = 125^\circ\!.155 \pm 1^\circ\!.355$ (the ψ dependence wraps around at $\pm 45^\circ$, so the actual value used is $35^\circ\!.155$) and $\iota = 62^\circ\!.17 \pm 2^\circ\!.20$.

There is reason to believe that the PWN orientation reflects that of the central pulsar, but in case this is not an accurate description we present results using both a uniform prior over all parameters, and using the restricted prior ranges. The MCMC only searches over the four main parameters and does not include errors on the pulsar position, frequency or frequency derivatives as these are negligible. The results are summarized in Table 3, where for the ellipticity and spin-down limit calculations a distance of 2 kpc was used. The orientation angle suggested by the restricted priors is slightly favorable in terms of the observable gravitational wave emission it would produce, and this allows us to set a better upper limit.

In Figure 5, we plot the result from model (1), with restricted priors, as an exclusion region on the moment of inertia–ellipticity plane. It can been seen that for all the allowed regions in moment of inertia we beat the spin-down limit.
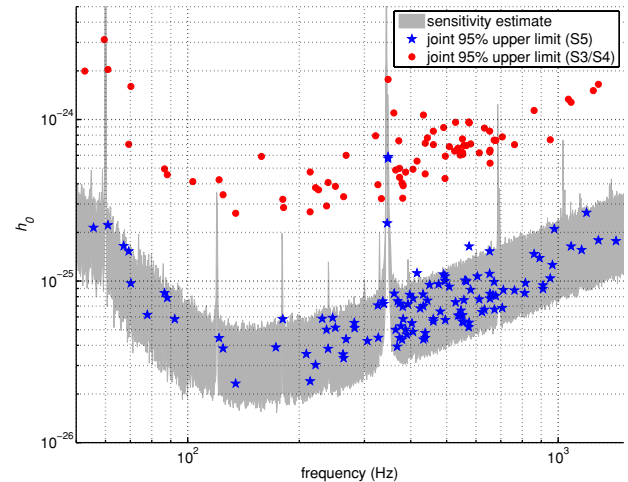

Figure 4. Gravitational wave amplitude upper limits are plotted over the estimated sensitivity of the search as defined by the gray band (see the text). Also plotted are the limits from the S3/S4 search.

(A color version of this figure is available in the online journal.)

If one assumes the Crab pulsar to have a moment of inertia at the upper end of the allowed range our result beats the spin-down limit by over an order of magnitude.

5.1.2. PSR J0537−6910

For pulsar J0537−6910, which has so far been timed only in X-rays, we rely on data from the *RXTE* satellite. This pulsar is young, has a high spin-down rate, and is a prolific glitcher, and therefore we require observations overlapping with our data to produce a coherent template. Middleditch et al. (2006) have published observations covering from the beginning of S5 up to 2006 August 21, during which time the pulsar was seen to glitch three times. Further observations have been made which span the rest of the S5 run and show another three glitches during this time. The epochs and parameters for the seven ephemeris periods overlapping with our data run are given in Table 2. For the first epoch there was no data for L1, so the joint result only uses H1 and H2 data. For the analyses using all the data (models 1 and 2) we have 474 days of H1 data, 475 days of H2 data, and 397 days of L1 data. Due to the glitches we perform parameter estimation for the same three models given above.

Table 2
Ephemeris Information for PSR J0537−6910

S. No.	Start–End (MJD)	ν (Hz)	$\dot{\nu}$ (Hz s^{-1})	$\ddot{\nu}$ (Hz s^{-2})	Epoch (MJD)
1.	53551–53687	62.000663106	$-1.994517 \times 10^{-10}$	11.2×10^{-21}	53557.044381976239
2.	53711–53859	61.996292178	$-1.993782 \times 10^{-10}$	8.1×10^{-21}	53812.224185839386
3.	53862–53950	61.995120229	$-1.994544 \times 10^{-10}$	9.6×10^{-21}	53881.096123033291
4.	53953–53996	61.993888026	$-1.995140 \times 10^{-10}$	9.6×10^{-21}	53952.687378384607
5.	54003–54088	61.992869785	$-1.994516 \times 10^{-10}$	2.2×10^{-21}	54013.061576594146
6.	54116–54273	61.990885506	$-1.994577 \times 10^{-10}$	8.1×10^{-21}	54129.540333159754
7.	54277–54441	61.988307647	$-1.994958 \times 10^{-10}$	7.7×10^{-21}	54280.918705402011

Note. The first four values are taken from Middleditch et al. (2006).

Table 3
Results of the Analysis for the Crab Pulsar, J0537−6910, and J1952+3252

Epoch	$h_0^{95\%}$		Ellipticity		$h_0^{95\%}/h_0^{\text{sd}}$	
	Uniform	Restricted[a]	Uniform	Restricted[a]	Uniform	Restricted[a]
			Crab pulsar			
Model (1)[b]	2.6×10^{-25}	2.0×10^{-25}	1.4×10^{-4}	1.1×10^{-4}	0.18	0.14
Model (2)[c]	2.4×10^{-25}	1.9×10^{-25}	1.3×10^{-4}	9.9×10^{-5}	0.17	0.13
1.	4.9×10^{-25}	3.9×10^{-25}	2.6×10^{-4}	2.1×10^{-4}	0.34	0.27
2.	2.4×10^{-25}	1.9×10^{-25}	1.3×10^{-4}	1.0×10^{-4}	0.15	0.13
			J0537−6910			
Model (1)[b]	2.9×10^{-26}	3.9×10^{-26}	8.9×10^{-5}	1.2×10^{-4}	1.0	1.3
Model (2)[c]	4.1×10^{-26}	4.6×10^{-26}	1.2×10^{-4}	1.4×10^{-4}	1.4	1.5
1.	9.1×10^{-25}	1.2×10^{-24}	2.8×10^{-3}	3.7×10^{-3}	31.2	41.2
2.	1.2×10^{-25}	1.5×10^{-25}	3.6×10^{-4}	4.6×10^{-4}	4.1	5.2
3.	1.4×10^{-25}	1.3×10^{-25}	4.2×10^{-4}	3.8×10^{-4}	4.7	4.3
4.	8.3×10^{-26}	1.1×10^{-25}	2.5×10^{-4}	3.3×10^{-4}	2.8	3.7
5.	1.4×10^{-25}	1.3×10^{-25}	4.1×10^{-4}	4.0×10^{-4}	4.7	4.6
6.	4.4×10^{-26}	5.8×10^{-26}	1.3×10^{-4}	1.8×10^{-4}	1.5	2.0
7.	4.9×10^{-26}	6.1×10^{-26}	1.5×10^{-4}	1.9×10^{-4}	1.7	2.1
			J1952+3252			
Model (1)[b]	2.5×10^{-25}	⋯	2.3×10^{-4}	⋯	2.0	⋯
Model (2)[c]	3.6×10^{-25}	⋯	3.3×10^{-4}	⋯	2.9	⋯
1.	4.7×10^{-25}	⋯	4.3×10^{-4}	⋯	3.8	⋯
2.	4.4×10^{-25}	⋯	4.0×10^{-4}	⋯	3.5	⋯

Notes.
[a] Uses observationally restricted priors on the orientation angle and polarization angle.
[b] Uses the full data set for a coherent analysis.
[c] Uses the full data set, but searches over an extra phase parameter at each glitch.

As with the Crab pulsar, there is also information on the orientation of J0537−6910 from model fits to its PWN (Ng & Romani 2008). These are used to set Gaussian priors on ψ and ι of $\psi = 131°\!.0 \pm 2°\!.2$ (equivalently 41°.0) and $\iota = 92°\!.8 \pm 0°\!.9$. We again quote results using uniform priors over all parameters and with these restricted priors. The distance used in the ellipticity and spin-down limits for J0537−6910 is 49.4 kpc. The results are summarized in Table 3. Using the restricted priors we obtain a worse upper limit on h_0 than for uniform priors. This is because the nebula suggests that the star has its spin axis perpendicular to the line of sight, and therefore the gravitational radiation is linearly polarized and the numerical strain amplitude is lower than average for a given strain tensor amplitude h_0.

In Figure 5, we again plot the result from model (1), with restricted priors, on the moment of inertia–ellipticity plane. It can be seen that the spin-down limit is beaten if we assume a moment of inertia to be 2×10^{38} kg m^2 or greater.

5.1.3. PSR J1952+3252

PSR J1952+3252 is another young pulsar with a high spin-down rate (although a couple of orders of magnitude less than for the Crab pulsar and J0537−6910)—it has spin parameters of $\nu = 25.30$ Hz and $\dot{\nu} = -3.73 \times 10^{-12}$ Hz s^{-1}. Jodrell Bank observations of this pulsar were made over the whole of S5, but it was observed to glitch at some point between 2007 January 1 and January 12. For both the pre- and post-glitch epochs, we have coherent timing solutions and again perform analyses as above. There are no constraints on the orientation of this pulsar, so we do not use any restricted priors. The results for this pulsar are given in Table 3. We reach about a factor of 2 above the spin-down limit using a distance of 2.5 kpc. The result from model (1) is also plotted on the moment of inertia–ellipticity plane in Figure 5. It can be seen that I_{38} just over 4, which is above the expected maximum allowable value, would be needed to beat the spin-down limit.
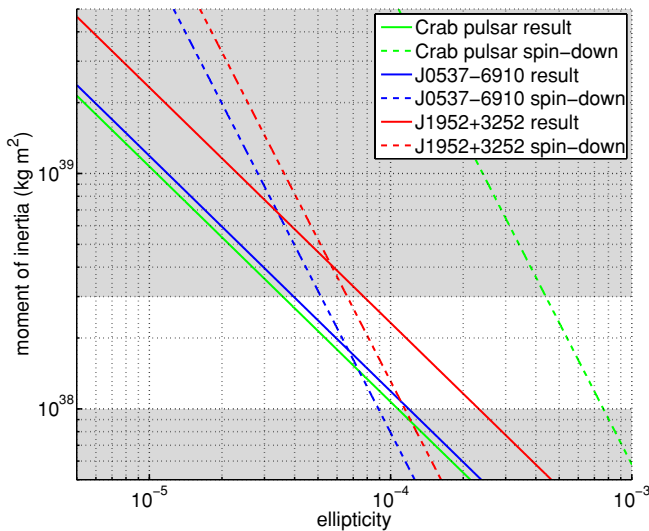
Figure 5. Results of the Crab pulsar, J0537−6910, and J1952+3252 analyses, and the spin-down limits, plotted on the moment of inertia–ellipticity plane. The results used are those from model (1) and with restricted priors on the angular parameters for the Crab pulsar and J0537−6910. Areas to the right of the diagonal lines are excluded. The shaded regions are those outside the theoretically predicted range of moments of inertia $I_{38} = 1–3$.

(A color version of this figure is available in the online journal.)

6. CONCLUSIONS

In this paper, we have searched for continuous gravitational waves from an unprecedented number of pulsars with unprecedented sensitivity, using coincident electromagnetic observations of many millisecond and young pulsars. Our direct upper limits have beaten the indirect limits (including the spin-down limit) for the Crab pulsar and are at the canonical spin-down limit for J0537−6910. For several more pulsars our upper limits are within roughly 1 order of magnitude of the spin-down limits, and therefore we expect a comparable search of Advanced LIGO and Virgo data to beat the latter.

For the Crab pulsar we improve upon the previous upper limit, which already beats the spin-down limit and other indirect limits; and we also provide results for different scenarios in which the signals may not be fully coherent over the run. By assuming that the observationally constrained priors on the angular parameters are correct we can limit the power output of the pulsar (see Abbott et al. 2008) to be less than ∼2% of the canonical spin-down luminosity.

Pulsar J0537−6910 is an interesting case due to its youth and glitchiness. Assuming that the gravitational wave signal phase is coherent with the X-ray pulses over glitches, our upper limit is within a few percent of the canonical spin-down limit for this pulsar. If we assume that the phase is incoherent over the glitches, then using the full data set our upper limit is ∼1.2 times the canonical spin-down limit. Even if we assume that none of the four main pulsar parameters remains coherent during a glitch (i.e., there is a major rearrangement in the star's structure) then the results from the final two epochs individually are still only approximately two times the spin-down limit. All of these direct upper limits are within the uncertainties of the spin-down limit, and (unlike the Crab) there is no firmly observed braking index and thus no substantially stricter indirect limit.

Pulsar J1952+3252 gets close to its spin-down limit, but even taking into account moment of inertia and distance uncertainties, probably would still just miss beating it. It does however make an exciting target for future runs.

Our observational upper limits on the ellipticities of the Crab and J0537−6910 are in the vicinity of 10^{-4}. Elastic deformations of this magnitude have been predicted as sustainable (Owen 2005; Haskell et al. 2007; Lin 2007; Knippel & Sedrakian 2009) not for normal neutron stars but only for exotic forms of crystalline quark matter (Xu 2003; Mannarelli et al. 2007). Such ellipticities could also be sustained by internal toroidal magnetic fields of order 10^{16} G depending on the field configuration, equation of state, and superconductivity of the star (Cutler 2002; Akgun & Wasserman 2007; Haskell et al. 2008; Colaiuda et al. 2008). Therefore, our observations have achieved the sensitivity to detect some of the more extreme possibilities, and have constrained the internal magnetic fields of the Crab and J0537−6910 to be less than of order 10^{16} G. However, it is important to be clear that the upper limits reported here do not constrain the properties of crystalline quark matter, because gravitational wave observations constrain the true ellipticity rather than the maximum ellipticity. This distinction was made clear in Owen (2005), but has not been properly enforced in more recent work (Lin 2007; Knippel & Sedrakian 2009). Also, while it is the case that, as anticipated by Haskell et al. (2007), the upper bounds on ellipticity reported here for some pulsars, notably J2124−3358, have pushed into a regime where elastic strains might support such deformations, detection was not expected, as such large ellipticities would conflict with the spin-down limit.

Recent work by Horowitz & Kadau (2009) suggests that the breaking strain of neutron star crusts may be an order of magnitude higher (10^{-1}) than the highest values (10^{-2}) previously used in estimates of maximum sustainable ellipticities. Their simulations are strictly applicable only to the outer crust (i.e., no neutron drip), but since the reason for the high breaking strain is very generic—the extreme pressure simply crushes away defects that contribute to early fracture—it may apply to the inner crust (the major contributor to ellipticity) as well. In that case, normal neutron stars could sustain ellipticities close to 10^{-5}, which is beyond the reach of the present search (for those stars where our results are at or near the spin-down limit) but would be accessible with data from advanced interferometers. If the high breaking strain holds for mixed phases in hybrid stars (which is not clear due to the increasing importance of the strong interaction at high densities), it would bring their maximum ellipticities estimated by Owen (2005) up an order of magnitude to about the 10^{-4} values achieved here.

In 2009 July, the LIGO 4 km detectors (featuring some upgraded systems and titled Enhanced LIGO) and the upgraded Virgo detector began their sixth and second science runs, respectively (S6 and VSR2). These upgrades aim to provide significantly better strain sensitivities than S5/VSR1. For LIGO these improvements will primarily be at frequencies greater than 40 Hz, but Virgo will improve at lower frequencies too and should outperform LIGO below about 40 Hz. LIGO and Virgo will closely approach and could potentially beat the spin-down limits not only for the Crab and J0537−6910 but for six more known pulsars: J1952+3252, J1913+1011, J0737−3039A, J0437−4715,[93] and the recently discovered J1747−2809 (Camilo et al. 2009) and J1813−1749 (Gotthelf & Halpern 2009). Below 40 Hz, Virgo could beat the spin-down limits for three more pulsars: the Vela pulsar, J0205+6449, and J1833−1034. Most of these 11 pulsars are young and may be

---

[93] This pulsar sits on a strong LIGO spectral noise line caused by the violin mode resonance of the suspension wires, so the required sensitivity may only be reachable with Virgo.

prone to large levels of timing noise and glitches. Therefore, to reach the best sensitivities it is essential to have radio and X-ray observations of these sources made in coincidence with the S6/VSR2 run. In particular, the extension of the *RXTE* satellite is crucial to our ability to perform targeted searches of J0537−6910 during this time of enhanced detector performance.

On a timescale of a few years, the Advanced LIGO and Virgo interferometers are expected to achieve strain sensitivities more than 10 times better for the pulsars in the current band, and will extend that band downward to approximately 10 Hz. Searches at such sensitivities will beat the spin-down limits from dozens of known pulsars and also enter the range of ellipticities predicted for normal neutron stars, improving the prospects for direct gravitational wave observations from these objects.

REFERENCES

Abbott, B., et al. 2004, Phys. Rev. D, 69, 082004
Abbott, B., et al. 2005, Phys. Rev. Lett., 94, 181103
Abbott, B., et al. 2007, Phys. Rev. D, 76, 042001
Abbott, B., et al. 2008, ApJ, 683, L45
Abbott, B., et al. 2009a, ApJ, 706, L203
Abbott, B., et al. 2009b, Rep. Prog. Phys., 72, 076901
Acernese, F., et al. 2008, Class. Quantum Grav., 25, 184001
Akgun, T., & Wasserman, I. 2007, MNRAS, 383, 1551
Bondarescu, R., Teukolsky, S. A., & Wasserman, I. 2009, Phys. Rev. D, 79, 104003
Brooks, S. P., & Roberts, G. O. 1998, Stat. Comput., 8, 319
Camilo, F., Ransom, S. M., Gaensler, B. M., & Lorimer, D. R. 2009, ApJ, 700, L34
Colaiuda, A., Ferrari, V., Gualtieri, L., & Pons, J. A. 2008, MNRAS, 385, 2080
Cordes, J. M., & Lazio, T. J. W. 2002, arXiv: astro-ph/0207156
Cutler, C. 2002, Phys. Rev. D, 66, 084025
Deller, A. T., Bailes, M., & Tingay, S. J. 2009, Science, 323, 1327
Dupuis, R. J. 2004, PhD thesis, Univ. of Glasgow
Dupuis, R. J., & Woan, G. 2005, Phys. Rev. D, 72, 102002
Goldreich, P., & Reisenegger, A. 1992, ApJ, 395, 250
Gotthelf, E. V., & Halpern, J. P. 2009, ApJ, 700, L158
Grote, H., & The LIGO Scientific Collaboration. 2008, Class. Quantum Grav., 25, 114043
Haskell, B., Andersson, N., Jones, D. I., & Samuelsson, L. 2007, Phys. Rev. Lett., 99, 231101
Haskell, B., Samuelsson, L., Glampedakis, K., & Andersson, N. 2008, MNRAS, 385, 531
Hobbs, G. B., Edwards, R. T., & Manchester, R. N. 2006, MNRAS, 369, 655
Horowitz, C. J., & Kadau, K. 2009, Phys. Rev. Lett., 102, 191102
Kaspi, V. M., Taylor, J. H., & Ryba, M. F. 1994, ApJ, 428, 713
Knippel, B., & Sedrakian, A. 2009, Phys. Rev. D, 79, 083007
Kramer, M., & Wex, N. 2009, Class. Quantum Grav., 26, 073001
Lin, L.-M. 2007, Phys. Rev. D, 76, 081502
Lindblom, L., Owen, B. J., & Ushomirsky, G. 2000, Phys. Rev. D, 62, 084030
Lyne, A. G., Pritchard, R. S., & Graham-Smith, F. 1993, MNRAS, 265, 1003
Lyne, A. G., Roberts, M. E., & Jordan, C. A. 2009, Jodrell Bank Crab Pulsar Monthly Ephemeris, http://www.jb.man.ac.uk/pulsar/crab.html
Manchester, R. N. 2008, in AIP Conf. Ser. 983, 40 Years of Pulsars: Millisecond Pulsars, Magnetars and More, ed. C. Bassa, Z. Wang, A. Cumming, & V. M. Kaspi (Melville, NY: AIP), 584
Manchester, R. N., Hobbs, G. B., Teoh, A., & Hobbs, M. 2005, AJ, 129, 1993
Mannarelli, M., Rajagopal, K., & Sharma, R. 2007, Phys. Rev. D, 76, 074026
Middleditch, J., Marshall, F. E., Wang, Q. D., Gotthelf, E. V., & Zhang, W. 2006, ApJ, 652, 1531
Ng, C.-Y., & Romani, R. W. 2008, ApJ, 673, 411
Ortolani, S., Barbuy, B., Bica, E., Zoccali, M., & Renzini, A. 2007, A&A, 470, 1043
Owen, B. J. 2005, Phys. Rev. Lett., 95, 211101
Owen, B. J., Lindblom, L., Cutler, C., Schutz, B. F., Vecchio, A., & Andersson, N. 1998, Phys. Rev. D, 58, 084020
Palomba, C. 2000, A&A, 354, 163
Umstätter, R., Meyer, R., Dupuis, R. J., Veitch, J., Woan, G., & Christensen, N. 2004, Class. Quantum Grav., 21, 1655
Veitch, J., Umstätter, R., Meyer, R., Christensen, N., & Woan, G. 2005, Class. Quantum Grav., 22, 995
Verbiest, J. P. W., et al. 2008, ApJ, 679, 675
Wu, Y., Matzner, C. D., & Arras, P. 2001, ApJ, 549, 1011
Xu, R. X. 2003, ApJ, 596, L59